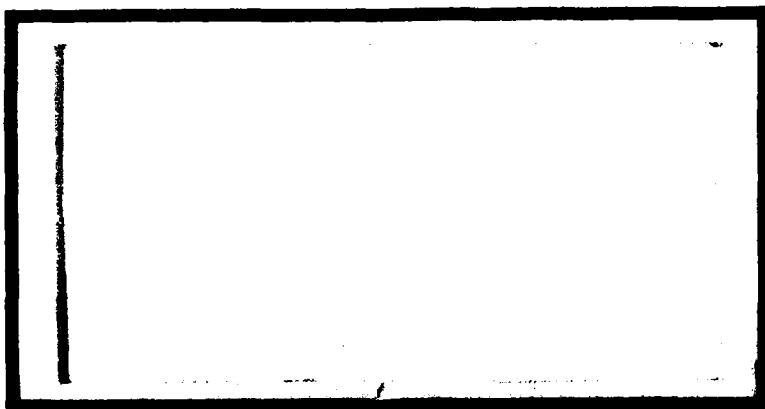


ADA 080411



Handwritten initials

LEFT



DDC FILE COPY

DDC
RECEIVED
FEB 7 1980
A

UNITED STATES AIR FORCE
AIR UNIVERSITY
AIR FORCE INSTITUTE OF TECHNOLOGY
Wright-Patterson Air Force Base, Ohio

DISTRIBUTION STATEMENT A
 Approved for public release
 Distribution Unlimited

80-2 5 249

14

AFIT/GE/EE/79-35

9) *Hastler's thesis,*

6) THRESHOLD OF THE VELOCITY GATE IN A
CONTINUOUS WAVE RADAR WITH CONICAL

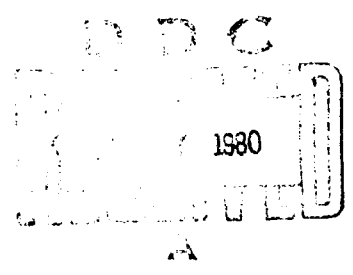
SCAN TRACKING -

THESIS

10) AFIT/GE/EE/79-35 Jonathan P. Sunray
2Lt USAF

11) *Dec 77*

12) *101*



Approved for public release; distribution unlimited.

012 225

AB

THRESHOLD OF THE VELOCITY GATE IN A CONTINUOUS
WAVE RADAR WITH CONICAL SCAN TRACKING

THESIS

Presented to the Faculty of the School of Engineering
of the Air Force Institute of Technology

Air Training Command
in Partial Fulfillment of the
Requirements for the Degree of
Master of Science

by

Jonathan P. Sunray, B.S.E.E.
2Lt USAF
Graduate Electrical Engineering

December 1979

Approved for public release; distribution unlimited.

Preface

This thesis report culminates six months of study of the velocity gate in a radar with conical scan angle tracking. The project arose out of an initial request from the Electronic Warfare Division of the Aeronautical Systems Division for some analysis of this type of radar that would aid in the understanding of effective electronic countermeasures. The importance of the velocity gate to the maintenance of accurate target tracking and the lack of available theoretical analysis to support its behavior prompted the effort that was devoted to the development of this report.

My sincere gratitude is extended to Capt. August Golden, my thesis advisor, and Lt. Col. Ron Carpinella, Major Joe Carl and Capt. Stan Robinson for helping me understand and learn much of the knowledge I gained as an AFIT student, and which I applied towards this thesis. In addition, I thank Dr. David Berri for initially suggesting the project.

I thank my dear wife Shiela for her support throughout this project and for coaxing me along when its end seemed an eternity away. And I express my appreciation to her for typing the numerous drafts.

Jonathan P. Sunray

Contents

	Page
Preface	ii
List of Figures	v
Abstract	vii
I. Introduction	1
Statement of the Problem	1
Objectives	3
Plan of Attack	3
II. Function of the Velocity Gate	5
Structure and Operation	6
III. Linear Analysis of the Velocity Gate	10
Steady State Tracking Model	10
Dynamic Tracking Model	15
IV. Noise Analysis of the Velocity Gate	25
Linear Model With Noise Included	28
Criterion for Validity of Linear Model	37
Defining a Noise Induced Threshold For The Velocity Gate	41
Determination of the Frequency Tracking Error Due to Noise	43
Example	59
Alternate Definition of Threshold	63
V. Conclusion	68
Summary	68
Recommendation	71
Bibliography	72
Appendix A: Response of an IF Filter to a Mis- tuned Carrier	74

Contents

	Page
Appendix B: Derivation of the Baseband Equivalent of an IF Filter	82
Vita	90

List of Figures

<u>Figure</u>		<u>Page</u>
1	Placement of Velocity Gate in a CONSCAN Receiver	5
2	Velocity Gate Block Diagram	7
3	Block Diagram of Velocity Gate Without AGC	11
4	Model of Velocity Gate For a Constant Input Offset Frequency	14
5	Linearized Dynamic Tracking Model of the Velocity Gate	23
6	Power Spectrums of $\underline{n}(t)$, $\underline{n}_I(t)$, and $\underline{n}_Q(t)$	27
7	Phasor Construction For Input Signal Plus Noise	29
8	Linear Model of the Velocity Gate For High CNR	32
9	Equivalent Filter Representation of Linear Model	33
10	Power Spectrum of Equivalent Noise Phase For High CNR	35
11	Probability $[Q_e(t) > 1]$ vs CNR_n	40
12	Block Diagram of Velocity Gate Without AGC	44
13	Relative Bandwidths of the IF Filter and the Noise Preceding it	49
14	Spectrums of $\hat{\underline{n}}(t)$, $\hat{\underline{n}}_I(t)$ and $\hat{\underline{n}}_Q(t)$	50
15	Phasor Diagram for Signal Plus Noise Prior to LD	52

List of Figures

<u>Figure</u>		<u>Page</u>
16	Equivalent Noise Phase at LD Input	53
17	Typical Fourier Transform of Voltage Spike .	55
18	CNR_n vs VCO RMS Frequency Deviation Due to Noise	62
19	CNR_n vs Probability $[f_o(t) > 300 \text{ Hz}]$	66
A-1	Depiction of IF Filter Magnitude and Phase Responses	75
A-2	Magnitude and Phase Responses of $H_{IF}^+(w+w')$ and $H_{IF}^-(w-w')$	75
A-3	Depiction of Narrowband Fourier Transforms	78
B-1	Magnitude and Phase Responses of $H_1(w)$ and $H_2(w)$	84

Abstract

A study is made of the behavior of the velocity gate in a continuous wave radar with conical scan tracking. Adapting the analysis of the frequency modulation feedback demodulator (FMFB), two linear models are developed for the velocity gate. The first deals with the gate's response to a static doppler frequency offset and the second deals with its response to a varying doppler frequency. The dynamic model also incorporates the presence of narrowband, Gaussian noise at the input to the gate. The phase tracking error of the gate due to noise is determined as a function of the carrier-to-noise ratio (CNR) in a bandwidth equal to the closed-loop noise bandwidth. Establishing the performance criterion to be the frequency tracking error, two definitions for the threshold of the gate are established. The first states the threshold occurs at the value of CNR for which the root-mean-square frequency tracking error due to noise exceeds half the 3db bandwidth of the IF filter within the gate. The second bases the threshold on the probability of the frequency error exceeding half the 3db bandwidth of the IF filter. Both definitions are applied to an example in which a second order velocity gate is considered.

THRESHOLD OF THE VELOCITY GATE IN A CONTINUOUS
WAVE RADAR WITH CONICAL SCAN TRACKING

I. Introduction

Statement of the Problem

A CW* radar with conical scan (CONSCAN) angle tracking sometimes employs a tunable, narrowband filter, called a velocity gate, to track the doppler-induced frequency variations of the received signal. The carrier to which the gate is locked is amplitude modulated by the antenna scanning. Accurate tracking of the carrier frequency enables the scan information to be detected after the gate with minimal distortion. However, tracking errors arise if noise or some other interference competes with the desired signal. The gate cannot distinguish the signal from the noise so it responds to the combination of the two; in doing so, the scan modulation may become distorted. When this distortion becomes serious enough to effectively destroy the scan modulation, the gate can be considered to have broken lock on the signal carrier or to have reached its threshold. Consequently, guidance information is denied

* continuous wave

to the radar antenna's servo loops.

From the standpoint of electronic countermeasures (ECM) a breaklock is desirable. Exploiting the possibility of a breaklock does not require any knowledge of the radar's scan frequency. In contrast, a technique which directly attacks the scan modulation, such as amplitude modulated jamming, must operate at the scan frequency to be effective. In view of the likelihood that the scan frequency is concealed from a jammer, this jamming technique becomes more difficult to apply. Thus, the vulnerability of the velocity gate in a CONSCAN radar is of interest to the radar designer as well as the ECM designer. For this reason, there is a need for theoretical analysis that predicts the behavior of the velocity gate when it tracks properly and when it breaks lock.

In researching this report no comprehensive analysis of a velocity gate was found. However, insight into its operation can be gleaned from a similar device, the frequency modulation feedback demodulator (FMFB) (ref 6,7). Both devices are feedback loops, designed to track the frequency variations of an input carrier. Their structures are almost identical and they operate on the same principles.

Objectives

This report was motivated by the lack of comprehensive analysis of the velocity gate in a CONSCAN radar. Although by no means comprehensive, this report provides insight into the behavior of the gate in the presence of noise and suggests certain performance criteria.

The first objective of the report is to adapt the analysis of the FMFB to the development of a linear model of the velocity gate. The model supports the tracking behavior of the gate under the condition of a large input carrier-to-noise ratio (CNR). Acquisition behavior will not be considered in this report.

The second objective is to analyze the effects of narrowband, Gaussian noise on the tracking performance of the gate. The intention is to show that loss of lock due to noise is really a probabilistic phenomenon, and based on a suitable criterion of performance, a threshold for the gate can be defined.

Plan of Attack

Following the introduction, section two of this report explains the purpose of the velocity gate in a radar with CONSCAN angle tracking. Also described will be its components and general operating method.

In the third section, frequency feedback principles will be applied in developing two linearized models of the gate when it is in its "locked state". This analysis will omit the effects of noise. The first model will describe the response to a static doppler frequency offset. The second model will deal with the response to a dynamic frequency input, arising from a varying target velocity. The applicability and validity of these models will be discussed.

The effects of noise on the dynamic tracking model will be discussed in section four where the analysis is made tractable and illustrative by several assumptions. Two cases will be considered, a high input CNR for which the linear model is valid, and a low CNR, which tends to invalidate the conditions upon which the linear model is based. Not predicted by the linear analysis is the presence of noise spikes in the feedback portion of the gate. The mechanism by which they occur will be described and their rate of occurrence will be shown to increase for decreasing CNR. Ultimately, they can lead to a loss of lock, as defined by some initially established criterion.

II. FUNCTION OF THE VELOCITY GATE

The placement of the velocity gate in a simplified CONSCAN receiver is shown in Figure 1.

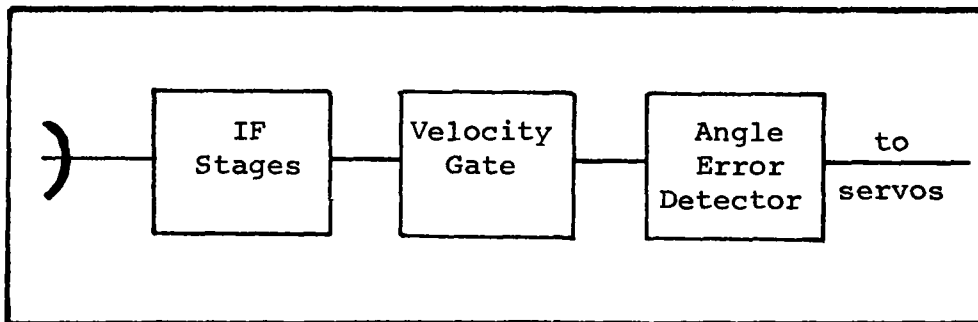


Figure 1. Placement of Velocity Gate in a CONSCAN Receiver

The gate functions like a narrowband predetection filter with tunable center frequency. Its bandwidth is considerably less than that required by a fixed bandpass filter before the angle detector. Such a fixed filter would require at least sufficient bandwidth to pass the expected range of doppler frequency shift associated with the scan modulated IF carrier*. However, the velocity gate responds to the instantaneous doppler offset frequency, effectively

* As an example of the expected range of doppler frequencies, consider a radar operating at 3 GHz. If the radial velocity between radar and target ranges between the extremes of 0 and 2000 miles per hour, the corresponding doppler shift ranges approximately between 0 and 18 KHz, respectively.

centering an internal IF filter on the target return. In reality, no tunable filter exists, but the actual operation (discussed next) is effectively the same. Theoretically, this internal IF filter requires just enough bandwidth to pass the scan modulation, but because of the finite response time of the gate, it is made wider. Nevertheless, the velocity gate filters substantially more noise than the otherwise fixed filter could.

Structure and Operation

Figure 2 presents a block diagram of the velocity gate. Included is an automatic gain control (AGC) device which is typically present in a radar receiver. The particular device shown maintains the DC level of the scan modulation impressed upon the IF carrier constant to prevent the saturation of components following the gate. Preceding the gate is a bandpass filter with a bandwidth B_i large enough to pass the maximum expected doppler shift and any sidebands produced by rapid changes in the target's velocity.

As mentioned above, the basic operational requirement of the gate is to track the input carrier frequency. This is accomplished by mixing the input with a reference signal from the voltage controlled oscillator (VCO). The frequency difference between this reference and the input is

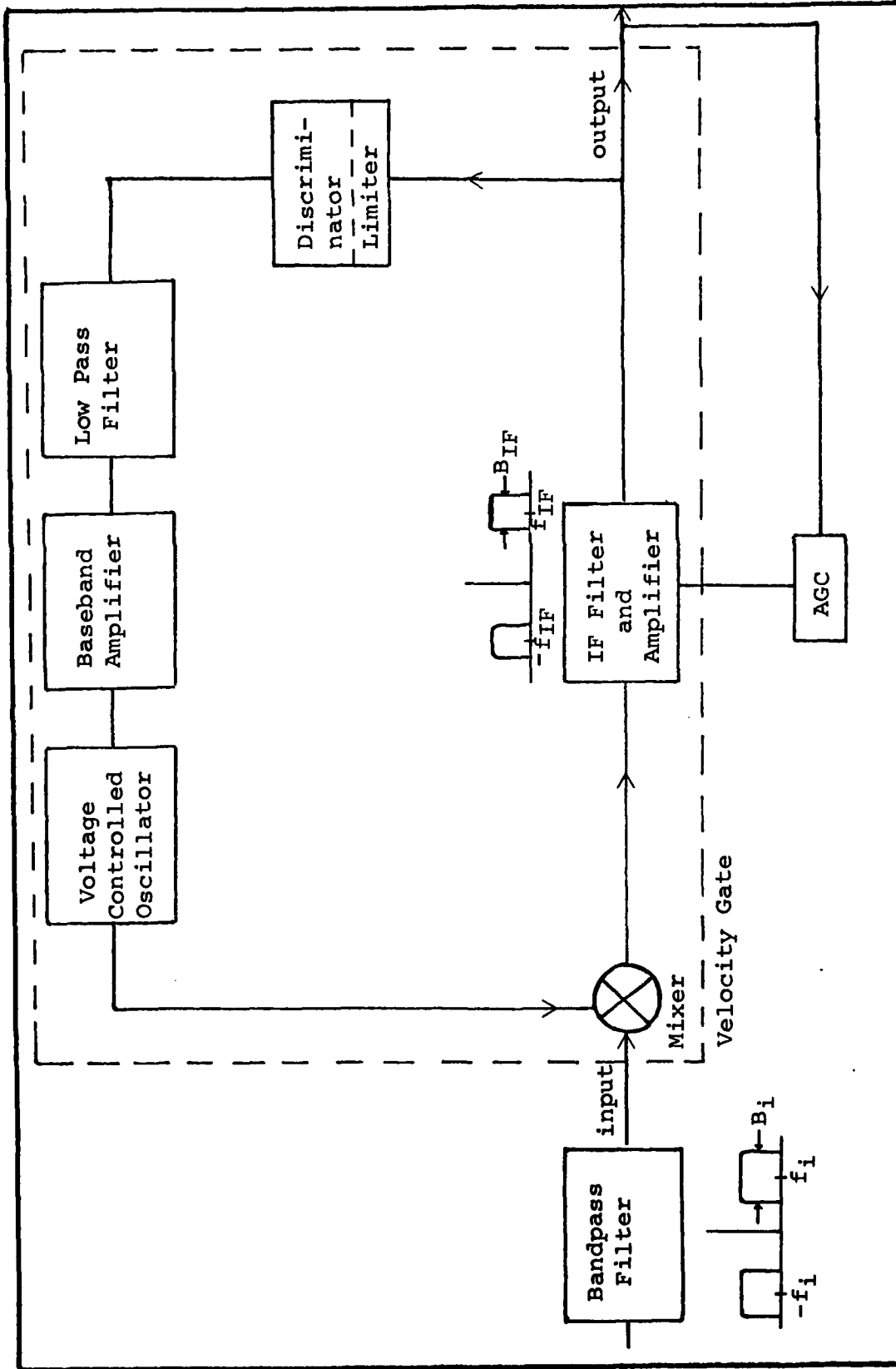


Figure 2. Velocity Gate Block Diagram

designed to be kept constant at the value of the IF center frequency. Thus, the difference-frequency component at the mixer output gets filtered by the IF to remove excess noise and other interference, while the sum-frequency component is blocked. The IF output will contain the scan modulation on a carrier ostensibly at the center frequency of the IF. Applying this signal to the limiter-discriminator (LD) yields a feedback voltage proportional to any frequency offset from the IF center. After being filtered and amplified, this voltage drives the VCO, whose output frequency deviates proportionally to the input voltage. The feedback action within the velocity gate forces the VCO to follow the input frequency. In this manner, the frequency error within the IF filter is driven towards zero, implying equilibrium of the gate.

Several assumptions are made here to help simplify the analysis of the velocity gate. The mixer is treated as a simple multiplier. The IF filter is considered to be symmetrical about its center frequency. It is assumed the limiter is perfect in the sense that it normalizes all signal amplitudes at the LD input. The AGC, therefore, can be neglected from the analysis because it will not affect the tracking performance of the gate. Supporting this is the

fact that the AGC action equally affects the carrier and noise so the CNR at the IF output is not changed. The discriminator output voltage is assumed to be a linear function of frequency for all frequencies of interest. Likewise, the VCO output frequency is a linear function of the voltage at its input.

Some of the above assumptions "idealize" the velocity gate to a certain extent. However, they pave the way for a more tractable analysis, as presented in the following sections.

III. LINEAR ANALYSIS OF THE VELOCITY GATE

The velocity gate is a nonlinear device, making a general analysis difficult. Fortunately, under certain conditions a linear analysis is possible, allowing the gate to be modeled as a linear feedback loop, to which conventional feedback theory can be applied. From the linear model the behavior of the gate when it is tracking properly, or "locked" to the input, can be described.

This section establishes the conditions which validate a linear analysis of the velocity gate. Two models will be developed based on these conditions. The first indicates the steady-state tracking response to a constant doppler offset of the input carrier. The second concerns the dynamic response to a varying input frequency. The inclusion of noise in these models is deferred until section IV.

Steady State Tracking Model

With reference to Figure 3, we consider an input signal of the form

$$a(t) = A(t)\sin(\omega_i t + \omega_d t) \quad (1)$$

$$A(t) = \text{scan modulation}$$

$$\omega_i = 2\pi f_i; f_i = \text{constant input carrier frequency (known)}$$

$$\omega_d = 2\pi f_d; f_d = \text{unknown doppler offset}$$

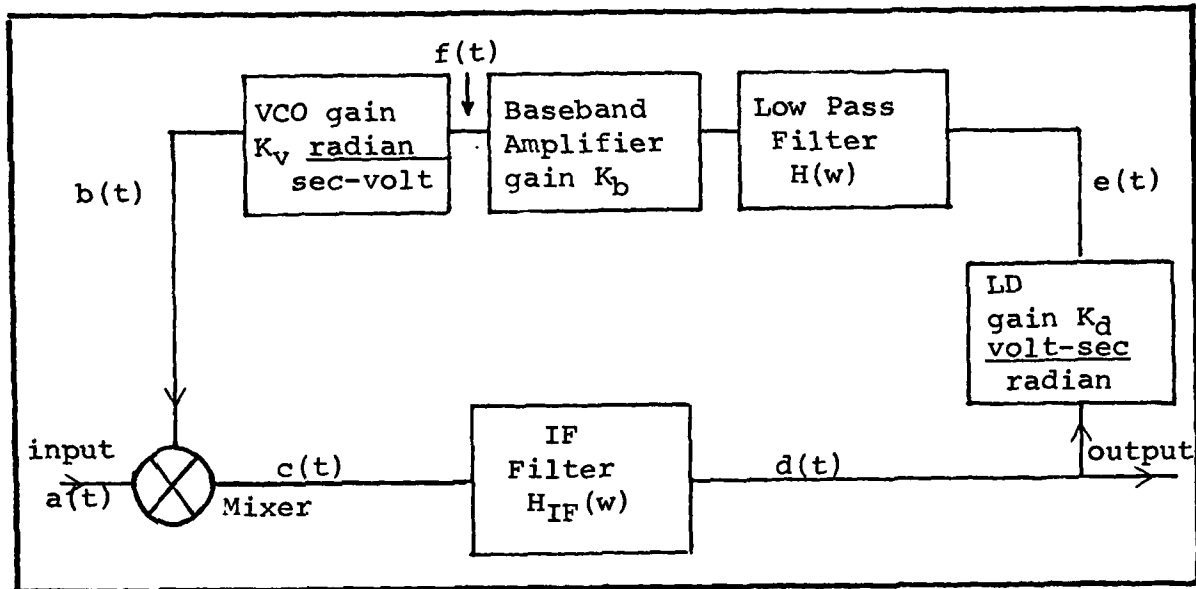


Figure 3. Block Diagram of Velocity Gate Without AGC

It is mixed with a reference signal from the VCO given by

$$b(t) = 2\cos(\omega_0 t + \omega_d' t) \quad (2)$$

$$\omega_0 = 2\pi f_0; f_0 = \text{VCO quiescent operating frequency}$$

$$\omega_d' = 2\pi f_d'; f_d' = \text{VCO frequency offset in response to gate input carrier offset}$$

Hence, we have at the mixer output the product

$$c(t) = a(t) \cdot b(t) \quad (3)$$

$$= A(t) \sin \left[(\omega_i - \omega_0) t + (\omega_d - \omega_d') t \right] \\ + A(t) \sin \left[(\omega_i + \omega_0) t + (\omega_d + \omega_d') t \right]$$

The VCO quiescent operating frequency, f_0 , is designed such that $(f_i - f_0) = f_{IF}$, which is the center frequency of the IF. Therefore, $(f_d - f_d') = \Delta f_d$ represents the frequency error in the IF filter.

Since the IF filter only passes the low frequency component, in Eq. (3), its output is

$$d(t) = K_e A(t) \sin(\omega_{IF} t + \Delta \omega_d t + \theta_e) \quad (4)$$

$$K_e = \text{IF gain at frequency } f_{IF} + \Delta f_d$$

$$\theta_e = \text{IF phase response at frequency } f_{IF} + \Delta f_d$$

Notice this voltage is also the output of the gate (we distinguish between the gate output after the IF filter and the loop output after the VCO). Insofar as the radar is concerned, the scan modulation $A(t)$ is the signal of interest. The above result implies that the bandwidth of $A(t)$ is small enough compared to the IF bandwidth to justify the assumption. Its few sidebands are undistorted by filtering action. Hereafter, as far as the IF filter is concerned, $A(t)$ will be treated as a constant.

The feedback signal in the gate is a voltage proportional to the frequency error within the IF filter. The LD performs the conversion from frequency to voltage after normalizing

the amplitude of the signal at its input. Effectively, the derivative of those terms within the sine argument in Eq. (4), other than $w_{IF}t$, is taken. Thus, we have the feedback voltage

$$e(t) = K_d \left[\frac{d}{dt} (\Delta w_d t + \theta_e) \right] \quad (5)$$

$$= K_d \Delta w_d$$

K_d = discriminator gain in $\frac{\text{volts-sec}}{\text{radian}}$

The low pass loop filter filters baseband noise and any transients. At the moment we are only concerned with the magnitude of its zero frequency ^{response}, given by $|H(0)|$. Therefore, the VCO input voltage is

$$f(t) = K_d K_b |H(0)| \Delta w_d \quad (6)$$

K_b = baseband amplifier gain

yielding the proportional output frequency deviation

$$w_d' = K_v K_d K_b |H(0)| \Delta w_d \quad (7)$$

K_v = VCO gain in $\frac{\text{radian}}{\text{sec-volt}}$

Using the knowledge that $\Delta w_d = w_d - w_d'$ and defining $K' = K_v K_d K_b |H(0)|$, EQ. (7) yields the following closed loop

transfer function for the VCO frequency response to a constant offset from the input carrier frequency

$$\frac{\omega_d'}{\omega_d} = \frac{K'}{1 + K'} \quad (8)$$

The frequency error transfer function is

$$\frac{\Delta\omega_d}{\omega_d} = \frac{\omega_d - \omega_d'}{\omega_d} = \frac{1}{1 + K'} \quad (9)$$

Eqs. (8) and (9) define the equivalent static frequency tracking model shown in Figure 4.

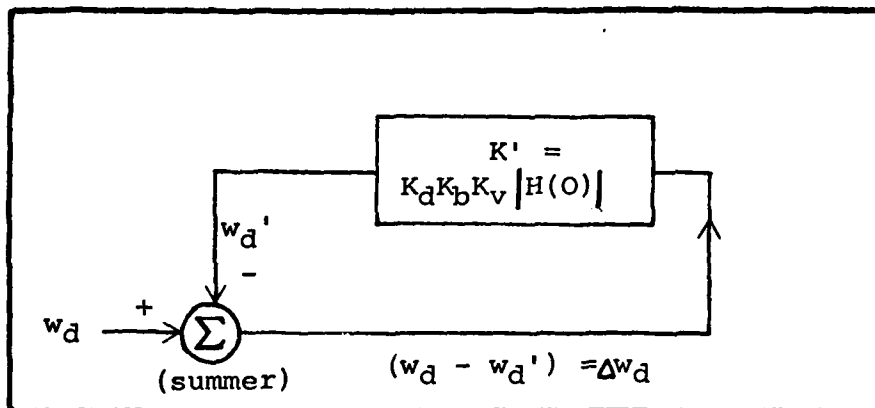


Figure 4. Model of Velocity Gate For a Constant Input Offset Frequency

It is evident the DC gain in the feedback path, given by K , determines how closely the VCO response matches a static input frequency offset (see Eq. 8). The larger the frequency error, the further the IF input signal will oper-

ate in the skirts of the IF filter. This is undesirable if the resulting attenuation exceeds the dynamic range of the AGC. In addition, as the gate attempts to track a fluctuating input doppler frequency, a carrier in the skirts of the IF filter may undergo excessive phase shifting, which can lead to an unstable condition of the loop. Yet, the maintenance of a small frequency error is not simply accounted for by placing a baseband amplifier of sufficient gain in the gate. Consideration must be given to the closed-loop noise bandwidth, which increases with the baseband gain. An alternative is to incorporate a perfect integrator into the low-pass loop filter. The resulting DC gain will be infinite, which implies the static frequency error is zero (see Eq. (9)). A perfect integrator does not exist but an active filter can approximate its characteristic (ref 8:9).

Dynamic Tracking Model

The static frequency tracking model assumes a static doppler offset of the carrier at the input to the gate. However, a static offset, indicative of a constant relative velocity, is not typical of a target moving relative to a tracking radar. More likely, the velocity will fluctuate about an average value due to maneuvers and attitude changes of the target. Accordingly, the scan-modulated carrier at the input to the gate will undergo doppler-induced frequency variations. There-

fore, a dynamic frequency tracking model is more representative of the velocity gate in actual operation.

Referring back to the block diagram of Figure 3, the gate input is now written

$$a(t) = A(t)\sin(\omega_i t + \omega_d t + \phi_i(t)) \quad (10)$$

Phase function $\phi_i(t)$ corresponds to the fluctuations in the carrier frequency discussed above. The VCO output is written

$$b(t) = 2\cos(\omega_o t + \omega_d' t + \phi_o(t)) \quad (11)$$

where the phase function $\phi_o(t)$ is the loop response to the input phase function. Our goal here is a linear transfer function relating $\phi_o(t)$ to $\phi_i(t)$, which would then yield the dynamic baseband model of the velocity gate.

The mixer output contains high and low frequency components. The low frequency component is the one passed by the IF filter, thus yielding the effective IF input

$$c(t) = A(t)\sin(\omega_{IF} t + \Delta\omega_d t + \phi_e(t)) \quad (12)$$

$$\omega_{IF} = \omega_i - \omega_o$$

$$\Delta\omega_d = \omega_d - \omega_d'$$

$$\phi_e(t) = \phi_i(t) - \phi_o(t)$$

Convolving this signal with the IF filter impulse response $h_{IF}(t)$ yields the IF (and velocity gate) output signal

$$d(t) = A(t)E(t)\sin(\omega_{IF}t + \Delta\omega_d t + \hat{\phi}_e(t)) \quad (13)$$

This particular response is derived in Appendix A, where $E(t)$ is shown to be an envelope function and $\hat{\phi}_e(t)$ the output phase function. Both are based on the input phase modulation and on the filter's impulse response. As before, the scan modulation is considered slowly varying compared to the IF bandwidth so that it passes through the filter without distortion.

To arrive at Eq. (13) in Appendix A the IF impulse response is expressed in the form

$$h_{IF}(t) = 2\text{Re} \left[\tilde{h}_L(t) e^{j(\omega_{IF} + \Delta\omega_d)t} \right] \quad (14)$$

Here, $\tilde{h}_L(t)$ is a complex envelope, not to be confused with the envelope function $E(t)$. It may seem unnecessary to reference the complex envelope to the frequency $\omega_{IF} + \Delta\omega_d$ since the filter is symmetrical about ω_{IF} . However, for a modulated input carrier of frequency $\omega_{IF} + \Delta\omega_d$, the representation in Eq. (14) is convenient for analytically obtaining the output.

The linear model of the velocity gate is actually a baseband model, representing the gate's tracking response for the input phase function $\phi_i(t)$ [Eq. (10)]. To determine the model, it is necessary to derive a baseband filter which has the same response as the IF filter to the phase function $\phi_e(t)$, given by Eq. (12).

The unwieldy expression for the phase function, $\hat{\phi}_e(t)$, derived in Appendix A, can be simplified to yield the equivalent baseband filter if $\phi_e(t)$ is much less than one radian. As derived in Appendix B, the resulting baseband filter is real and defined by its transfer function

$$H_{LP}(w) = \text{Re} \left[\frac{\tilde{H}_L(w)}{\tilde{H}_L(0)} \right] \quad (15)$$

Here, $\tilde{H}_L(w)$ is the Fourier transform of the complex envelope $\tilde{h}_L(t)$. Having determined Eq. (15), the impulse response of the baseband equivalent filter is simply the inverse Fourier transform of $H_{LP}(w)$, denoted by $h_{LP}(t)$. Therefore, if the input phase function has a magnitude less than one radian, the output phase function is given by

$$\hat{\phi}_e(t) = \phi_e(t) * h_{LP}(t), \quad (16)$$

where " * " denotes convolution. The significance of this expression is that the baseband equivalent filter, defined by the impulse response $h_{LP}(t)$, can be incorporated into a linear model of the velocity gate. Provided the above condition on $\phi_e(t)$ holds, the response of this filter in the baseband realm is equivalent to the IF filter's response.

Recalling that the complex envelope $\tilde{h}_L(t)$ of the IF filter is a function of the offset frequency, $\Delta\omega_d$, (see Eqs. (A-4) and (A-5) in Appendix A), $h_{LP}(t)$ will also have such dependence. However, it seems reasonable to assume that for a slight offset from the IF center frequency, the input carrier would be filtered not much differently than a carrier with no frequency offset. Consequently, the baseband equivalent can be approximated by the particular equivalent derived for $\Delta\omega_d = 0$. Indeed, this is the case, as shown by Klapper and Frankle (ref 7:63-64). For a single pole IF filter, they experimentally determined that $\Delta\omega_d$ can extend up to half the 3db bandwidth of the IF filter and the baseband equivalent would not change significantly. One would expect the range of acceptable mistuning for a higher order filter to be more restricted since its transfer characteristic will have a sharper rolloff after the 3db frequency than the single pole. Restricting the frequency error in the IF also

helps to avoid operation in the skirts of the filter, which can induce excess phase shifts in the output (ref 6:25, 7:64).

In summary, to develop a linear model of the velocity gate using the baseband equivalent of the IF passband response, the phase modulation prior to the IF must be less than one radian. For the appropriate value of the IF carrier offset $\Delta\omega_d$, the baseband equivalent transfer function is then given by Eq. (15). Given the further condition of an IF carrier offset within the IF filter 3db bandwidth, the baseband equivalent filter is determined by Eq. (15), but applied to the case $\Delta\omega_d = 0$. Furthermore, if the IF mid-band gain and phase shift are one and zero, respectively, referring to Eq. (B-1) in Appendix B, we see the baseband equivalent is simply given by the passband response, shifted and centered at zero frequency. This particular response is conventionally denoted as the low pass equivalent of the IF filter (ref 11:122). In addition, the envelope function $E(t)$ in Eq. (13) is equal to one, as indicated by Eq. (B-12).

With $\hat{\phi}_e(t) = \phi_e(t) * h_{LP}(t)$ (Eq. (16) and $E(t) = 1$, Eq. (13) can be simplified to yield

$$d(t) = A(t) \sin(\omega_{IF}t + \Delta\omega_d t + (\phi_e(t) * h_{LP}(t))) \quad (17)$$

The discriminator output is a function of the instantaneous

frequency deviation from the IF center. Hence,

$$\begin{aligned} e(t) &= K_d \left[\frac{d}{dt} (\Delta w_d t + (\phi_e(t) * h_{LP}(t))) \right] \\ &= K_d \left[\Delta w_d + \frac{d}{dt} (\phi_e(t) * h_{LP}(t)) \right] \end{aligned} \quad (18)$$

After baseband filtering and amplification of the discriminator output, the VCO input voltage can be written

$$\begin{aligned} f(t) &= K_b K_d \left[\left[\Delta w_d + \frac{d}{dt} (\phi_e(t) * h_{LP}(t)) \right] * h(t) \right] \\ &= K_b K_d \Delta w_d |H(0)| + K_b K_d \left[\frac{d}{dt} (\phi_e(t) * h_{LP}(t)) * h(t) \right] \end{aligned} \quad (19)$$

where $h(t)$ is the impulse response of the low pass filter.

The first term in Eq. (19) is the feedback voltage corresponding to the static input frequency offset w_d . The second term is the feedback voltage corresponding to the input phase function $\phi_i(t)$ and is the term we are interested in here.

Because the VCO output frequency is directly proportional to the input voltage, the corresponding phase will be proportional to the integral of the voltage. Therefore, the loop phase response to the input phase function is

$$\begin{aligned}\phi_o(t) &= K_v K_b K_d \left[\int_{-\infty}^t \left[\frac{d}{dt} (\phi_e(t) * h_{LP}(t)) * h(t) \right] dt \right] \quad (20) \\ &= K [\phi_e(t) * h_{LP}(t) * h(t)] ,\end{aligned}$$

where K is defined as $K_v K_b K_d$.

With $\phi_e(t) = \phi_i(t) - \phi_o(t)$, and using the Laplace operator s , the linearized dynamic model of the velocity gate has transfer function

$$\begin{aligned}\frac{\phi_o(s)}{\phi_i(s)} &= \frac{K H_{LP}(s) H(s)}{1 + K H_{LP}(s) H(s)} \quad (21) \\ &\triangleq G(s)\end{aligned}$$

The error transfer function is

$$\begin{aligned}\frac{\phi_e(s)}{\phi_i(s)} &= \frac{\phi_i(s) - \phi_o(s)}{\phi_i(s)} = \frac{1}{1 + K H_{LP}(s) H(s)} \quad (22) \\ &\triangleq 1 - G(s)\end{aligned}$$

The model described by the transfer functions in Eqs. (21) and (22) is pictured in Figure 5. In order to preserve the functional characteristic of the discriminator and VCO, they are depicted as a differentiator and integrator, respectively.

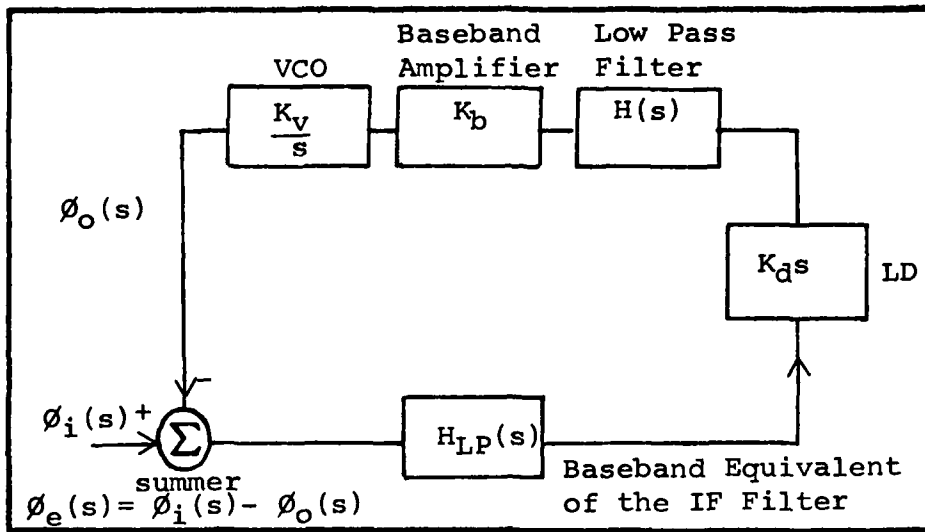


Figure 5. Linearized Dynamic Tracking Model of the Velocity Gate

Understandably, the linear model of the velocity gate is identical to the linear model of the FMFB (ref 7:53) since both devices have the same structures. It is important to note, however, that as a frequency demodulator, the FMFB does not have to contend with an input carrier as greatly mistuned as that which the velocity gate encounters due to the predominance of the doppler effect. In addition, the bandwidth of the filters within the FMFB will generally be much greater than that required by those within the velocity gate due to the larger extent of the FM signal spectrum.

The reader may note that if the baseband equivalent filter, the differentiator and the low-pass filter in the

velocity gate are combined into one overall loop filter, the model presented in Figure 5 resembles the linear model of a phase locked loop (PLL) (ref 16:129). However, some differences between the two devices are worth mentioning. For one, the PLL would require either a limiter or an AGC to normalize the amplitude of the input signal, thus making the closed-loop response insensitive to signal amplitude (ref 3:219, 226; 9:56), as is the case with the velocity gate. Furthermore, the PLL is designed to be phase coherent with the input signal, and attempts to minimize the phase error between the VCO and the input. As will be seen, the performance criterion of the velocity gate does not have to be as strict, for the purpose of the gate is to maintain a small enough frequency error in the IF filter to keep the scan modulation out of its skirts.

IV. NOISE ANALYSIS OF THE VELOCITY GATE

The preceding analysis of the velocity gate must be adapted to a noisy environment. As in all communication systems, noise in the velocity gate contributes to performance loss. This means the gate's ability to track the frequency variations of the input signal becomes less effective as the input noise power rises. Although the noise is a random process, that portion within the bandwidth of the gate is not distinguished from the signal so the tracking response is due to the combination of the two. Depending on what performance criterion is chosen, the gate will have a noise-induced threshold, below which performance is unacceptable. Considered in this section will be the tracking behavior of the velocity gate for a relatively low and high carrier-to-noise ratio (CNR). The analysis is intended to suggest a possible performance criterion which can aid in defining a noise-induced threshold.

Recall from section three that the linear model of the velocity gate is based on the conditions of the frequency error and phase error within the IF filter being small. Violation of these conditions due to noise is possible and reduces the accuracy of the linear model in representing the behavior of the gate. This does not necessarily mean the gate

has broken lock or that the scan modulation is distorted beyond utility, for these conditions are subject to interpretation. However, it should be evident that the noise competes with the signal and tends to increase the tracking error. This error increases as the CNR decreases.

The analysis presented here assumes the input noise to the gate is a Gaussian stationary process. The bandpass filter preceding the gate (see Figure 3) is considered to have a bandwidth B_i considerably less than its mid-band frequency. This justifies a narrowband representation for the noise process (ref 14:254) as follows

$$\underline{n}(t) = \underline{n}_I(t)\cos w_i t - \underline{n}_Q(t)\sin w_i t \quad (23)$$

$\underline{n}(t)$ = narrowband input noise process

$\underline{n}_I(t)$ = in-phase component of $\underline{n}(t)$

$\underline{n}_Q(t)$ = quadrature component of $\underline{n}(t)$

$w_i = 2\pi f_i$, f_i = mid-band frequency of bandpass filter preceding velocity gate

In the nomenclature of this report, a line below a function of time implies the function is a random process. Each of $\underline{n}(t)$, $\underline{n}_I(t)$ and $\underline{n}_Q(t)$ have a zero mean value and their variances are equal. The in-phase and quadrature components are

uncorrelated lowpass processes with identical autocorrelation functions. Their power spectrums are given as follows

$$S_I(f) = S_Q(f) = \begin{cases} \frac{N_0 \text{ watts}}{\text{Hz}} & |f| < \frac{B_i}{2} \\ 0 & |f| > \frac{B_i}{2} \end{cases} \quad (24)$$

The power spectrum of $\underline{n}(t)$ is

$$S(f) = \begin{cases} \frac{N_0}{2} \frac{\text{watts}}{\text{Hz}} & f_i - \frac{B_i}{2} \leq |f| \leq f_i + \frac{B_i}{2} \\ 0 & \text{all other frequencies} \end{cases} \quad (25)$$

These power spectrums are pictured in Figure 6.

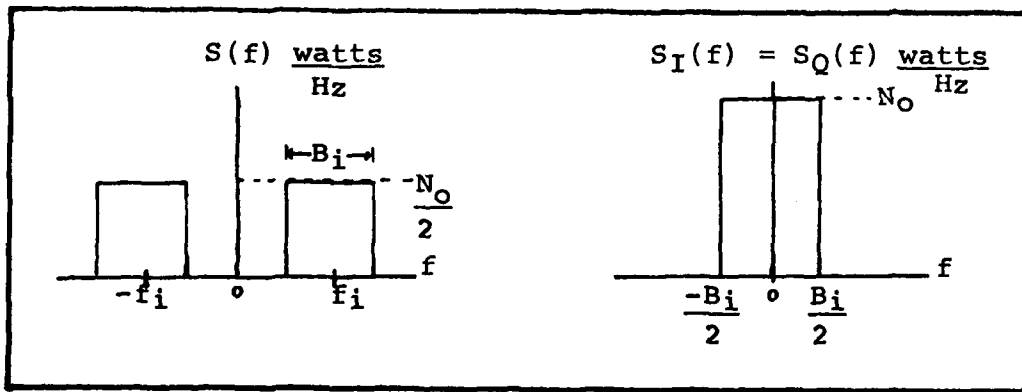


Figure 6. Power Spectrums of $\underline{n}(t)$, $\underline{n}_I(t)$ and $\underline{n}_Q(t)$

Combining Eqs. (10) and (23), the overall input signal plus noise is

$$a(t) = A(t)\sin(w_i t + w_d t + \phi_i(t)) \quad (26)$$
$$+ n_I(t)\cos w_i t - n_Q(t)\sin w_i t$$

Linear Model With Noise Included

The linear model of the velocity gate in Figure 5 yields the VCO output phase variation to an input phase variation. As mentioned earlier, this phase variation corresponds to the doppler-induced frequency variations of the signal carrier. Provided the model remains valid, it can also be used to find the gate response to the overall signal plus noise input given by Eq. (26). This is conveniently done if the noise is represented as an equivalent phase modulation of the scan-modulated carrier. In this manner, the net input phase function will be a random process, having a deterministic component due to the doppler-induced frequency variations and a random noise component.

With the aid of a phasor diagram, the signal plus noise can analytically combined. The construction is shown in Figure 7, where it is indicated the signal phasor has a

magnitude $A(t)$ and is referenced to the same frequency as the in-phase and quadrature noise components. The signal phasor thus has a phase

$$\theta_s(t) = \omega_d t + \phi_i(t) \quad (27)$$

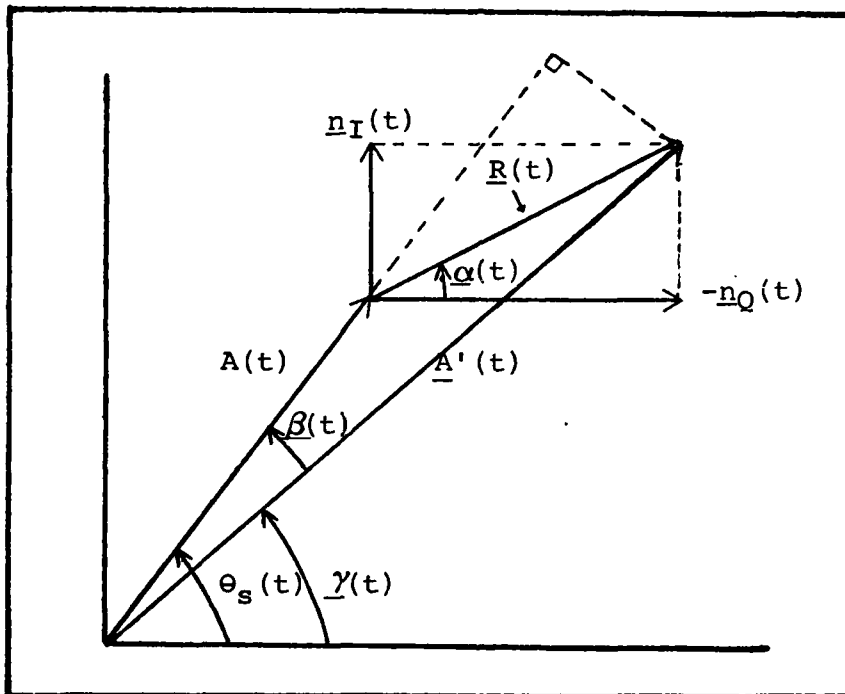


Figure 7. Phasor Construction For Input Signal Plus Noise

From Figure 7 the following relationships are evident:

$$\underline{n}(t) = \sqrt{|\underline{n}_I(t)|^2 + |\underline{n}_Q(t)|^2} \sin(\omega_i t + \underline{\alpha}(t)) \quad (28)$$

$$\doteq \underline{R}(t) \sin(\omega_i t + \underline{\alpha}(t)), \text{ where}$$

$$\underline{\alpha}(t) = \tan^{-1} \left[\frac{|\underline{n}_I(t)|}{-|\underline{n}_Q(t)|} \right] \quad (29)$$

$$\underline{\beta}(t) = \tan^{-1} \left[\frac{\underline{R}(t) \sin(\theta_s(t) - \underline{\alpha}(t))}{\underline{A}(t) + \underline{R}(t) \cos(\theta_s(t) - \underline{\alpha}(t))} \right] \quad (30)$$

$$\underline{\gamma}(t) = \theta_s(t) - \underline{\beta}(t) = \omega_d t + \phi_i(t) - \underline{\beta}(t) \quad (31)$$

$$\underline{A}'(t) = \sqrt{(\underline{A}(t) + \underline{R}(t) \cos(\theta_s(t) - \underline{\alpha}(t)))^2 + (\underline{R}(t) \sin(\theta_s(t) - \underline{\alpha}(t)))^2} \quad (32)$$

The magnitude of the resultant phasor $\underline{A}'(t)$ and the phase $\underline{\gamma}(t)$ correspond to the magnitude and phase, respectively, of the input into the velocity gate. Thus, Eq. (26) can be equivalently written

$$\underline{a}(t) = \underline{A}'(t) \sin(\omega_i t + \omega_d t + \phi_i(t) + \underline{\beta}(t)) \quad (33)$$

Here, $\underline{\beta}(t)$ is the equivalent phase modulation of the signal carrier caused by noise.

Considering for the moment a high CNR, for example, $\underline{A}(t) \gg \underline{R}(t)$, two approximations are possible. From Eq. (32) $\underline{A}'(t) \approx \underline{A}(t)$ and from Eq. (30)

$$\begin{aligned}
\beta(t) &\approx \frac{R(t)\sin(w_d t + \phi_i(t) - \alpha(t))}{A(t)} & (34) \\
&= - \left[\frac{\underline{n}_I(t)\cos(w_d t + \phi_i(t)) + \underline{n}_Q(t)\sin(w_d t + \phi_i(t))}{A(t)} \right] \\
&\doteq \phi_{n_i}(t)
\end{aligned}$$

Therefore, Eq. (33) yields

$$\underline{a}(t) = A(t)\sin(w_i t + w_d t + \phi_i(t) + \phi_{n_i}(t)) \quad (35)$$

It should be emphasized that $\phi_{n_i}(t)$ is a representation for the equivalent phase modulation of the signal carrier due to noise. It is convenient to present the noise in this manner because the response of the loop is a phase modulation of the VCO output signal, given by $\phi_o(t)$ in Eq. (11). The velocity gate treats the input noise as if it were a random signal component and attempts to track its variations. Consequently, the VCO phase is comprised of a random process added to a deterministic component due to the actual input signal phase. With a large CNR one would expect the gate to still behave linearly, for the phase tracking error induced by noise should be small. However, even for a large CNR, there is a probability, although

small, of a noise spike which momentarily might induce a large enough phase error to invalidate the linear model. Keeping this in mind, the linear model of Figure 5 can still be modified to include the presence of noise, as shown in Figure 7. Note the VCO phase modulation is a random process.

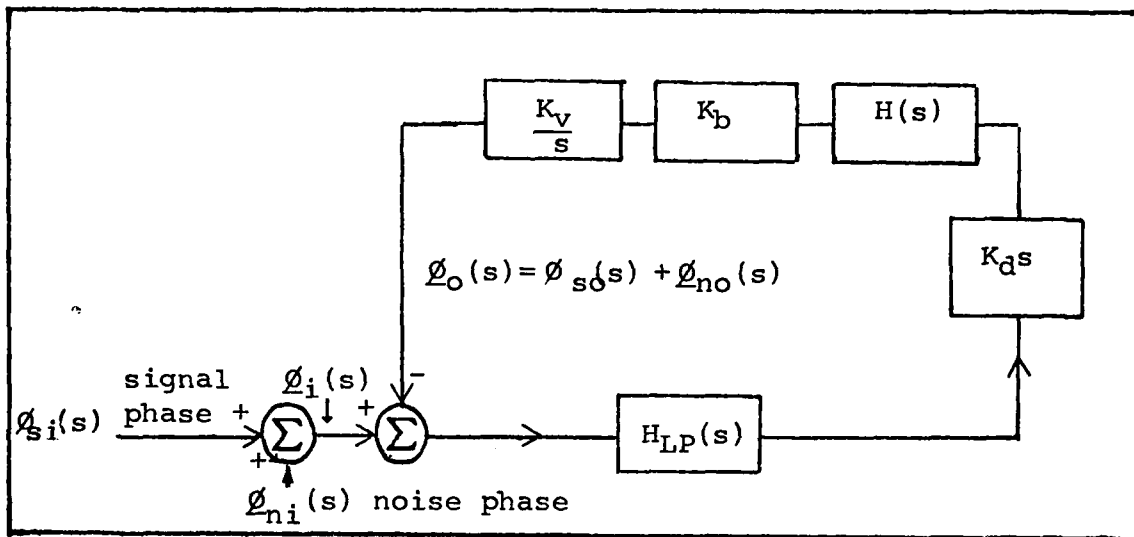


Figure 8. Linear Model of the Velocity Gate For High CNR

The VCO output phase $\phi_o(t)$ is a random process comprised of a deterministic signal component $\phi_{so}(t)$ and a random noise component $\phi_{no}(t)$. Since the linear model defines the equivalent linear filter of Figure 8, the output noise statistics can be found as a function of the input statistics. The equivalent filter has a transfer function given by Eq. (21).

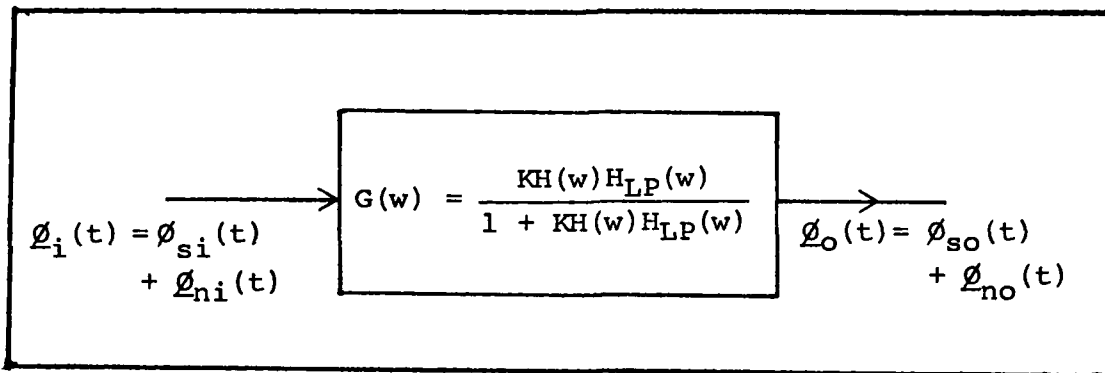


Figure 9. Equivalent Filter Representation of Linear Model

For purposes of example and simplicity, assume the input signal phase $\phi_{si}(t)$ is zero. The only implication of this is that the VCO phase will have a deterministic component of zero but the random component will be unaffected.

Thus,

$$\phi_i(t) = \phi_{ni}(t) = \frac{-\underline{n}_I(t)\cos w_d t - \underline{n}_Q(t)\sin w_d t}{A} \quad (36)$$

The scan modulation $A(t)$ is assumed to be slowly varying with respect to the noise terms. Thus, its expected value A has been used in Eq. (36). It is evident the expected value of $\phi_{ni}(t)$ is zero. Its autocorrelation function, given by $R_{\phi_i}(\tau)$, is derived as follows, where "E" stands for expected value. Recall, the noise components $\underline{n}_I(t)$ and $\underline{n}_Q(t)$

have zero cross correlation and the same autocorrelation function, i.e., $R_{nI}(\tau) = R_{nQ}(\tau)$.

$$\begin{aligned}
 R_{\phi_i}(\tau) &= E \left[\phi_{ni}(t) \phi_{ni}(t - \tau) \right] & (37) \\
 &= E \left[\frac{1}{A^2} (\underline{n}_I(t) \cos w_d t - \underline{n}_Q(t) \sin w_d t) \cdot \right. \\
 &\quad \left. (\underline{n}_I(t - \tau) \cos w_d(t - \tau) - \underline{n}_Q(t - \tau) \sin w_d(t - \tau)) \right] \\
 &= \frac{R_{nI}(\tau)}{A^2} (\cos w_d t) (\cos w_d(t - \tau)) \\
 &\quad + \frac{R_{nQ}(\tau)}{A^2} (\sin w_d t) (\sin w_d(t - \tau)) \\
 &= \frac{R_{nI}(\tau)}{A^2} \cos w_d \tau,
 \end{aligned}$$

where the identity $(\cos(a)\cos(b) + \sin(a)\sin(b)) = \cos(a - b)$ has been used to obtain the final result. The input noise power spectrum is the Fourier transform of Eq. (37) and is pictured in Figure 9.

The output power spectrum is given in terms of the squared magnitude of the linear system function $G(j\omega)$ (ref 12:347).

$$S_{\phi_o}(f) = S_{\phi_i}(f) |G(j\omega)|^2 \quad (38)$$

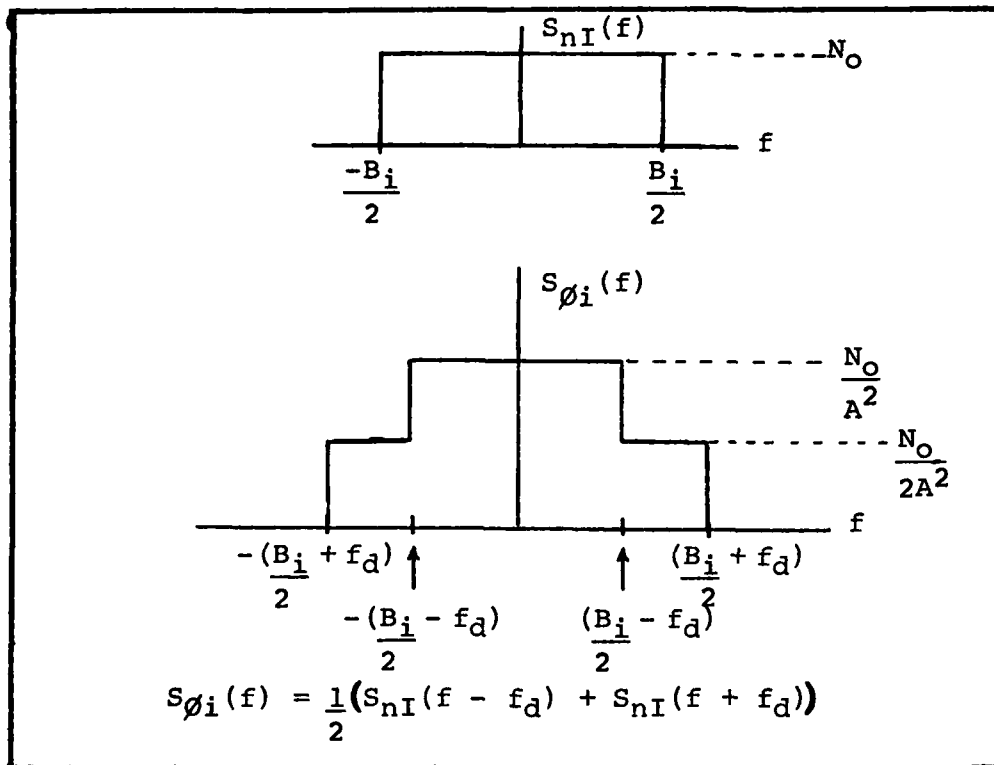


Figure 10. Power Spectrum of Equivalent Noise Phase For High CNR

From Eq. (38) it should be clear the VCO output phase due to noise will be a random process. If an input signal phase $\phi_{si}(t)$ were present, the gate would track it as well as the noise. The VCO output due to noise would effectively cause a phase jitter about the deterministic signal response. The mean-squared value of this jitter increases as the input noise spectral density N_0 , increases. Consequently, the phase tracking error of the gate will increase. A similar effect is observed with the FMFB (ref 6:21) and PLL (ref 8:21). The

mean squared value of the jitter is determined by

$$E[\phi_{no}^2(t)] = 2 \int_0^{\infty} S_{\phi_i}(f) |G(j\omega)|^2 df \quad (39)$$

Notice for the input power spectrum shown in Figure 10, which holds for zero signal modulation, the integration in Eq. (39)

consists of two portions. One lies over the range $f = 0$ to $f = \frac{(B_i - f_d)}{2}$. The other lies over the range $f = \frac{(B_i - f_d)}{2}$

to $f = \frac{(B_i + f_d)}{2}$, where all other frequencies yield zero

contribution to the integral. Yet, if the noise bandwidth of the velocity gate is within the frequency band $\frac{(B_i - f_d)}{2}$,

only the spectrum over this range significantly contributes to the integral in Eq. (39). Recall the bandwidth B_i of the bandpass filter preceding the gate is larger than the maximum expected doppler shift so that it passes the sidebands which are present when the target velocity changes abruptly.

Thus, $\frac{B_i - f_d}{2}$ would be on the order of several thousand

hertz, even for the largest static doppler shift f_d . By de-

sign, the noise bandwidth of the gate is likely to be much less. Considering the input phase power spectral density to be $\frac{N_0}{A^2}$ over the bandwidth of the gate, the mean square

phase deviation of the VCO is written

$$\begin{aligned}
 E\left[\varphi_{no}^2(t)\right] &= \frac{2N_o}{A^2} \int_0^{\infty} |G(j\omega)|^2 d\omega & (40) \\
 &= \frac{2N_o}{A^2} |G(0)|^2 B_n
 \end{aligned}$$

where B is the noise bandwidth of the gate, defined

$$B_n = \frac{\int_0^{\infty} |G(j\omega)|^2 d\omega}{|G(0)|^2} \quad (41)$$

Criterion for Validity of Linear Model

With regard to the linear model of Figure 8, it was mentioned above that the input noise can invalidate the small phase error requirement. The probability of this occurring for a high CNR is small enough to justify the model under this circumstance. However, the model becomes less representative of the gate for decreasing CNR. Thus, associated with the linear model is a validity criterion based on the probability the phase error exceeds one radian. It is shown here that this probability increases as the CNR decreases.

The loop phase error is defined as the difference between the input signal phase and the VCO output phase. It

is important to note that the input signal phase is given solely by the phase function $\phi_{si}(t)$. Although we have defined an equivalent input phase due to noise, this was only done for the convenience of determining the VCO output phase via the linear model. In contrast, however, the loop output phase is defined as the overall phase process out of the VCO. Thus, for zero input signal phase the loop phase error $\phi_e(t)$ is simply the loop response to the equivalent noise phase given in Eq. (36). Hence, after the second summer in Figure 8, the loop phase error is $\phi_e(t) = \phi_i(t) - \phi_o(t) = -\phi_{no}(t)$. Hereafter, the negative sign will be neglected. Although the absence of a signal phase is not typical, the analysis presented here should be useful for establishing a lower bound on the phase error for a particular CNR.

Since for a high CNR the input phase process is Gaussian, then by virtue of the linearity of the gate's transfer function, the VCO output phase process is Gaussian. Its probability density function, therefore, is written

$$f_{\phi_{no}}(\phi_{no}) = \frac{1}{\sqrt{2\pi}\sigma_{no}} \exp \left[-\frac{1}{2} \frac{\phi_{no}^2}{\sigma_{no}^2} \right] \quad (42)$$

The variance of $\phi_{no}(t)$ is defined σ_{no}^2 and is given by Eq. (40)

since the output noise process has a zero mean. Assuming the equivalent model has a DC gain of unity, $|G(0)| = 1$ and

$$\sigma_{no}^2 = \frac{2N_0B_n}{A^2} \quad (43)$$

The CNR in a bandwidth equal to the noise equivalent bandwidth is defined

$$CNR_n = \frac{A^2}{4N_0B_n} = \frac{1}{2\sigma_{no}^2} \quad (44)$$

For an unmodulated carrier, at any particular time, t , probability $[\varphi_e(t) > 1] = \text{probability}[\varphi_{no}(t) > 1]$. Using Eq. (39),

$$\text{probability} [|\varphi_e(t)| > 1] = 2 \int_{-\infty}^{\infty} \frac{1}{\sqrt{2\pi}\sigma_{no}} \exp \left[-\frac{1}{2} \frac{\varphi_{no}^2}{\sigma_{no}^2} \right] d\varphi_{no} \quad (45)$$

The factor of two implies positive and negative phase errors are considered. With the change of variables $y = \frac{\varphi_{no}}{\sqrt{2}\sigma_{no}}$, Eq.

(41) yields

$$\begin{aligned} \text{probability} [|\varphi_e(t)| > 1] &= 2 \int_{-\infty}^{\infty} \frac{1}{\sqrt{2}\sigma_{no}} \frac{1}{\sqrt{\pi}} \exp [-y^2] dy \quad (46) \\ &= \text{erfc} \left(\frac{1}{\sqrt{2}\sigma_{no}} \right) \\ &= \text{erfc} \left(\sqrt{CNR_n} \right) \end{aligned}$$

Here, "erfc" represents the error function complement defined as

$$\text{erfc}(x) = \frac{2}{\sqrt{\pi}} \int_x^{\infty} \exp[-y^2] dy \quad (47)$$

Eq. (42) is plotted in Figure 11.

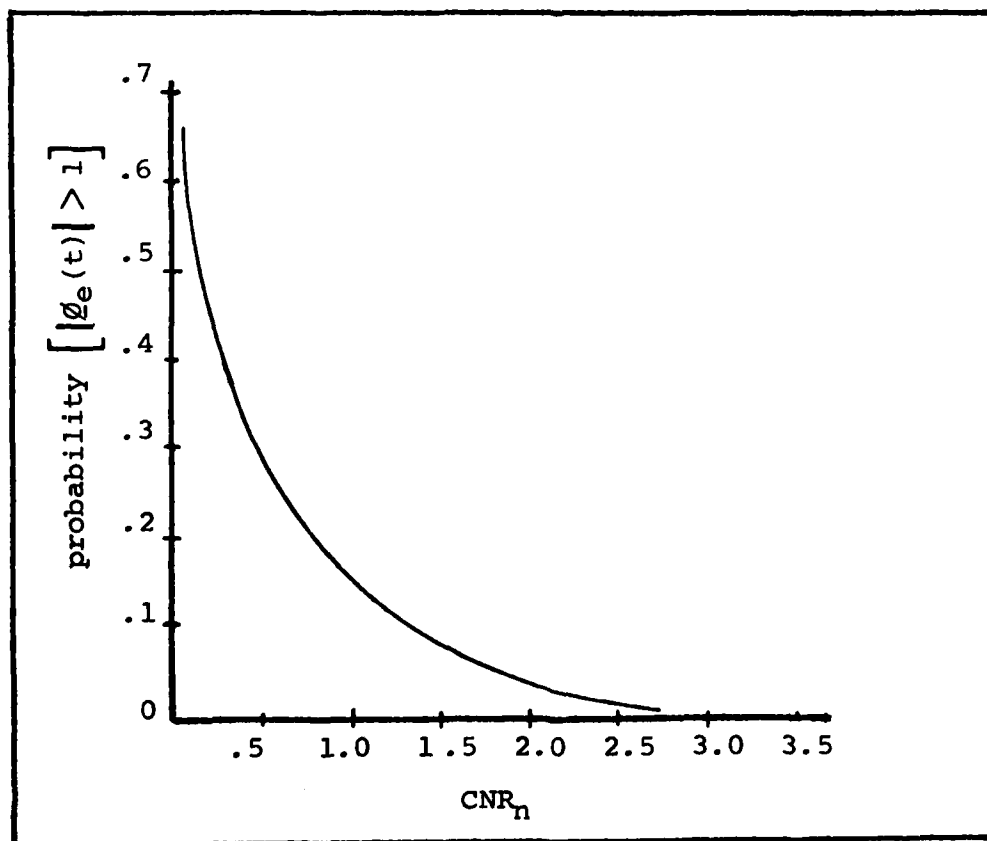


Figure 11. Probability [|g_e(t)| > 1] vs CNR_n

The reader will no doubt notice an inherent contradiction in the foregoing analysis. The equivalent phase due to noise, given by Eq. (36), is only valid when the CNR is large enough to justify the approximation made in arriving at the expression. Yet, no such restriction was placed on the CNR in obtaining Figure 11, where the equivalent noise phase was considered to be Gaussian, irrespective of the CNR. For a large CNR, Figure 11 could certainly be used to predict the accuracy of the linear model. But it must be kept in mind that the linear analysis does not accurately indicated the behavior of the gate for a lower CNR. However, the inaccuracy of the linear model only implies the phase tracking error is larger than one. A criterion based on the frequency tracking error would seem to be more significant since the purpose of the gate is to center the scan-modulated carrier within the IF filter. Nevertheless, the linear analysis applied to finding the phase error provides a useful benchmark for quantifying the performance of the velocity gate in the presence of noise. Indeed, it indicates the need for a more specific description of the noise and its influence on the gate.

Defining A Noise-Induced Threshold For The Velocity Gate

With regard to communication systems, the usage of the word "threshold" is directed at the condition when receiver

performance is no longer satisfactory. Accordingly, a noise-induced threshold is associated with a value of signal-to-noise ratio, referenced to some point in the receiver. Yet, the definition of threshold is arbitrary because it depends on how a user defines "unsatisfactory performance". For example, an FM demodulator is stated to be at its threshold when detected noise is one decibal more than that predicted by a linear analysis of the device (ref 14:322). The point here is that some measurable criterion must be established for distinguishing between good and bad performance.

We would expect that a threshold could also be defined for the velocity gate. Recall the purpose of the gate is to maintain the scan-modulated IF carrier within the IF pass-band with as little distortion as possible. The frequency error between the instantaneous carrier frequency and the IF center frequency is a useful measure of how well the gate is tracking. A non zero error is realistic because the gate has a finite response time to the input carrier frequency variations. But too much error will push the IF carrier (and the scan information) into the skirts of the IF filter, where it is subject to more amplitude and phase distortion than nearer the center frequency. Sufficient noise power accompanying the input signal can dominate the response of the gate so that the accurate signal tracking will be thwarted.

The implication is that the signal carrier at the IF input will fluctuate randomly between such a broad frequency range that the scan modulation will be pushed into the skirts of the filter and distorted.* But the distortion could be minimized if the tracking error is small enough to confine the signal carrier to the relatively flat passband around the IF filter's center frequency. Therefore, with the frequency tracking error as a performance criterion let us define the threshold to be reached when the root-mean-square frequency (RMS) error exceeds half the IF filter's 3db bandwidth. Some of the arbitrariness of this definition is removed in a subsequent section where the probability that the frequency error is greater than the 3db bandwidth of the IF filter is determined.

Determination of the Frequency Tracking Error Due to Noise

As mentioned in the introduction, the velocity gate has a structure very similar to a frequency demodulator with feedback (FMFB). The following analysis will be adapted

* The frequency tracking error can also be caused by an interfering carrier transmitted by a jammer, and swept in frequency through the passband of the gate. If the interference overrides the signal and is tracked, the gate will effectively break lock on the signal. Such a technique is conventionally called "velocity gate pulloff".

from the threshold analysis of the FMFB (ref 1:155,160, 14:359-361, 16:290,291).

A block diagram of the velocity gate, as presented in Figure 3, is reproduced here for convenience.

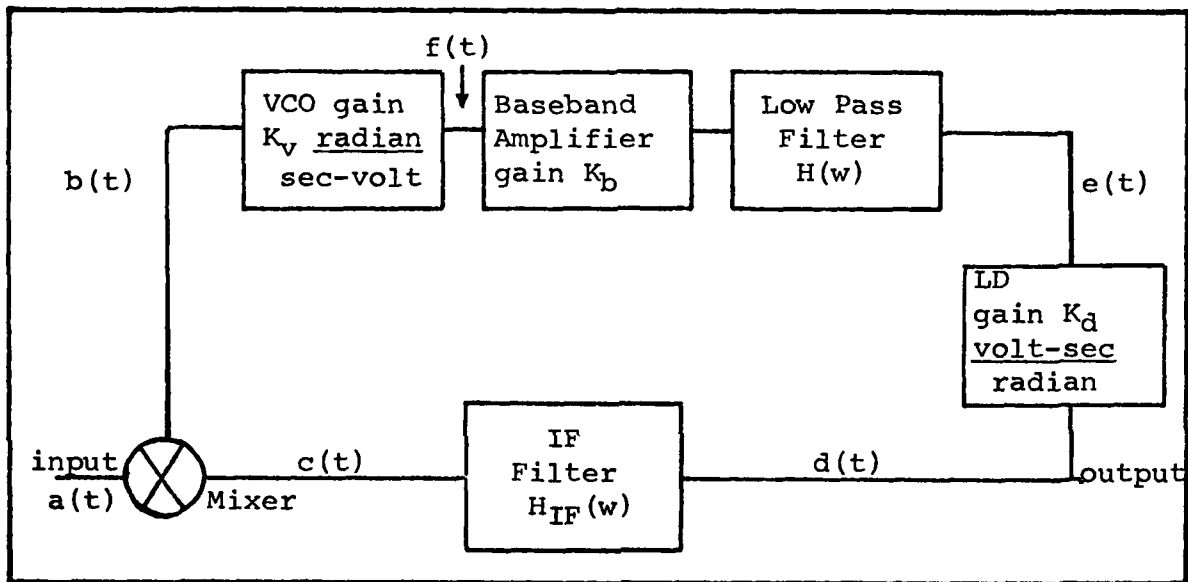


Figure 12. Block Diagram of Velocity Gate Without AGC

No dynamic signal phase will be considered. Thus, with only a constant doppler offset, the input to the gate from Eq. (26) is

$$\begin{aligned} \underline{a}(t) = & A(t)\sin(w_i t + w_d t) \\ & + \underline{n}_I(t)\cos w_i t - \underline{n}_Q(t)\sin w_i t \end{aligned} \quad (48)$$

The dynamic frequency response of the VCO will be due to the voltage $f(t)$ induced by noise. This voltage is produced by two mechanisms. The first occurs when the average input CNR is large. As presented earlier, the gate can be modeled as a linear filter with the input noise expressed as an equivalent input phase. The VCO input voltage due to this linear filtering mechanism will be a Gaussian process since the equivalent input phase process is Gaussian. The second mechanism occurs when the noise at the input to the LD momentarily rises above the signal and the equivalent noise phase at that point changes abruptly. Since the noise amplitude is described probabilistically there exists the possibility of this event. As a consequence, a voltage spike may be produced by the discriminator, with the result that the total noise power at the input to the VCO is increased. In the FM demodulator it is the occurrence of these spikes which causes a threshold (ref 14:323). The number of spikes per time interval increases as the CNR prior to the discriminator decreases.

The voltage at the VCO input produces a proportional frequency deviation at its output. Our concern is with the dynamic VCO output frequency due to noise and not with the static frequency response due to the fixed doppler offset f_d . Per the discussion in Section III, we assume there is suffi-

cient DC gain in the velocity gate so that the static frequency tracking error is small compared to the IF bandwidth. Thus, the significant frequency tracking error will be caused by noise. The objective is to determine the RMS frequency deviation of the VCO caused by the linearly filtered noise and the noise caused by the spiking.

Let us first consider the VCO frequency produced by linearly filtering the equivalent input phase process. Recall the power spectrum of the VCO phase is

$$S_{\phi_0}(f) = S_{\phi_i}(f) |G(j\omega)|^2 \quad (49)$$

where $S_{\phi_i}(f)$ is the spectrum of the input phase process and $|G(j\omega)|$ is the magnitude of the closed-loop transfer function of the linear model. The derivative of the stationary, Gaussian phase process yields the corresponding frequency process. If the autocorrelation of the phase process is $R_{\phi_0}(\tau)$, the autocorrelation of the frequency process is $\frac{-d^2}{d\tau^2} R_{\phi_0}(\tau)$

(ref 12:317). Hence, the VCO frequency process has a power spectrum given by

$$\begin{aligned} S_{f_0}(f) &= -(j\omega)^2 S_{\phi_i}(f) |G(\omega)|^2 \\ &= \omega^2 S_{\phi_i}(f) |G(\omega)|^2 \end{aligned} \quad (50)$$

With reference to Figure 10, the assumption is made again that the noise bandwidth of the gate is mostly in the frequency band $\frac{B_i}{2} - f_d$. Therefore the spectral density in the band is assumed to contribute entirely to the power of the frequency process. The mean squared value of the VCO output frequency due to linear filtering of the input noise process is

$$\begin{aligned}
 E \left[f_o^2(t) \right] &= \frac{2N_o}{A^2} \int_0^{B_n} w^2 df & (51) \\
 &= \frac{8\pi^2 N_o B_n^3}{3A^2} \\
 &= \frac{2\pi^2 B_n^2}{3 \text{ CNR}_n}
 \end{aligned}$$

where CNR_n is defined by Eq. (44) and is the carrier-to-noise ratio with the noise power defined in a bandwidth equal to the closed loop noise bandwidth.

Now let us consider the second source of frequency error; that is, the spiking phenomenon. As will be shown later, the occurrence of voltage spikes after the LD is a function of the CNR, before the LD. We thus turn our attention to finding an expression for the CNR at this particular point in the gate.

The VCO signal is

$$b(t) = 2\cos(\omega_0 t + \omega_d' t + \phi_{no}(t)) \quad (52)$$

Recall $\phi_{no}(t)$ is the phase process corresponding to the VCO random frequency and ω_d' is the static frequency tracking response.

Mixing with the input signal given by Eq. (48), and omitting the component which does not pass through the IF, yields the effective IF input,

$$\begin{aligned} c(t) = & A(t)\sin(\omega_{IF}t + \Delta\omega_d t + \phi_{no}(t)) \quad (53) \\ & + \underline{n}_I(t)\cos(\omega_{IF}t - \omega_d' t + \phi_{no}(t)) \\ & - \underline{n}_Q(t)\sin(\omega_{IF}t - \omega_d' t + \phi_{no}(t)) \end{aligned}$$

Assume the IF filter is ideal in the sense that its frequency response is given by a pair of bandpass rectangles of bandwidth B_{IF} and centered at $f = \pm f_{IF}$. This allows the IF output to be easily determined in an illustrative manner without complicating the analysis. Since the bandpass filter preceding the velocity gate (Figure 2) is greater than the largest expected doppler frequency shift, it is fair to say it is much greater than the noise equivalent bandwidth of the gate and even the bandwidth of the gate's IF filter. Thus, the noise processes $\underline{n}_I(t)$ and $\underline{n}_Q(t)$ vary much more rapidly than the VCO phase process $\phi_{no}(t)$. Consequently, they can be

considered independent from $\varnothing_{no}(t)$ (ref 3:155). In addition, although the noise spectrum will be significantly mistuned from the IF center frequency (by f_d' ; see Eq. (53)), its flat power spectrum will extend across the IF passband. This spectrum will be as wide as the bandwidth B_i of the filter preceding the gate. But the extent of the mistuning, which is indicative of the doppler shift of the gate input carrier, will be less than B_i . A depiction of the situation is presented in Figure 13.

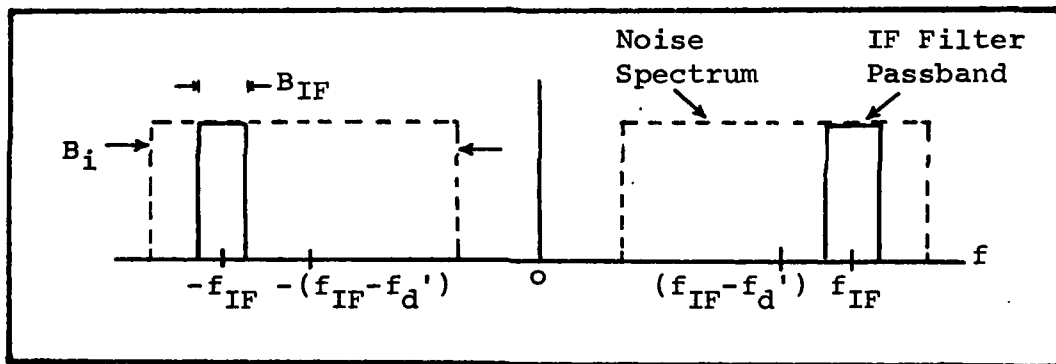


Figure 13. Relative Bandwidths of the IF Filter and the Noise Preceding It

The noise at the input to the IF filter completely fills its bandwidth. Since this bandwidth is small compared to f_{IF} , the output noise can be considered narrowband and written in the form

$$\hat{n}(t) = \hat{n}_I(t) \cos w_{IF}t - \hat{n}_Q(t) \sin w_{IF}t \quad (54)$$

Here, $\hat{n}_I(t)$ and $\hat{n}_Q(t)$ are the in-phase and quadrature, low-pass noise components after the IF filter. Their spectrums, as well as the spectrum of $\hat{n}(t)$, are depicted in Figure 14.

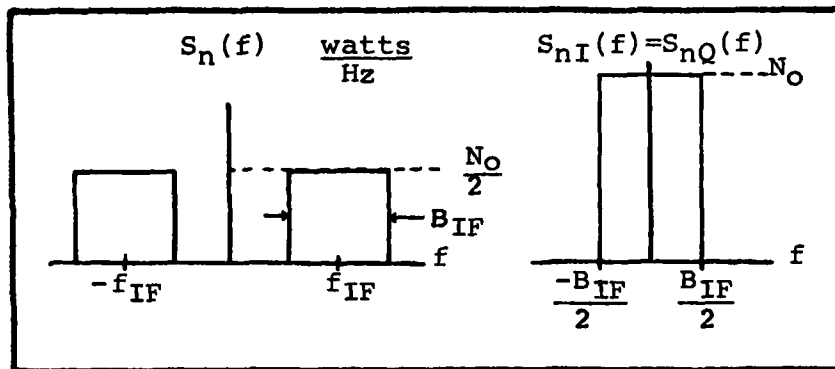


Figure 14. Spectrums of $\hat{n}(t)$, $\hat{n}_I(t)$ and $\hat{n}_Q(t)$

After the IF filter, the signal plus noise is written

$$\underline{d}(t) = A(t)\sin(\omega_{IF}t + \Delta\omega_d t) \quad (55)$$

$$+ \hat{n}_I(t)\cos(\omega_{IF}t) - \hat{n}_Q(t)\sin(\omega_{IF}t)$$

The CNR after the IF filter is also the CNR at the output of the velocity gate. It is given by the expression

$$CNR_{IF} = \frac{A^2}{2N_0 B_{IF}} \quad (56)$$

where, the mean value of the scan modulation A has been used as the carrier amplitude.

The noise in Eq. (55) can be considered an equivalent phase modulation, $\hat{\beta}(t)$, of the signal carrier and a phasor diagram similar to the one in Figure 7 can be constructed. Thus, the input into the LD can be written

$$\underline{d}(t) = \hat{A}'(t) \sin(\omega_{IF}t + \Delta\omega_d t + \hat{\beta}(t)), \quad (57)$$

where $\hat{A}'(t)$ is a random envelope (normalized by the limiter).

For $\text{CNR}_{IF} \gg 1$ the signal phasor has a magnitude A which is much larger than the noise phasor random magnitude $\hat{R}(t)$ (see Eq. (28)). Adding the signal and noise phasors vectorially yields a resultant phasor with magnitude $\hat{A}'(t)$. Since $\hat{R}(t) \ll A$, the tip of the resultant phasor will never wander far from the end point of the signal phasor. In Figure 15a the dotted line indicates a possible path for the tip of the resultant phasor. One can see the equivalent noise phase $\hat{\beta}(t)$ is small.

As the CNR decreases, the average magnitude of the noise phasor will increase relative to the signal phasor. As shown in Figure 15b, when $\hat{R}(t)$ is comparable to A there exists the possibility that the resultant phasor can completely encircle the origin. There is always a slight chance of this occurring even with a large CNR, but the probability increases drastically as the CNR is lowered.

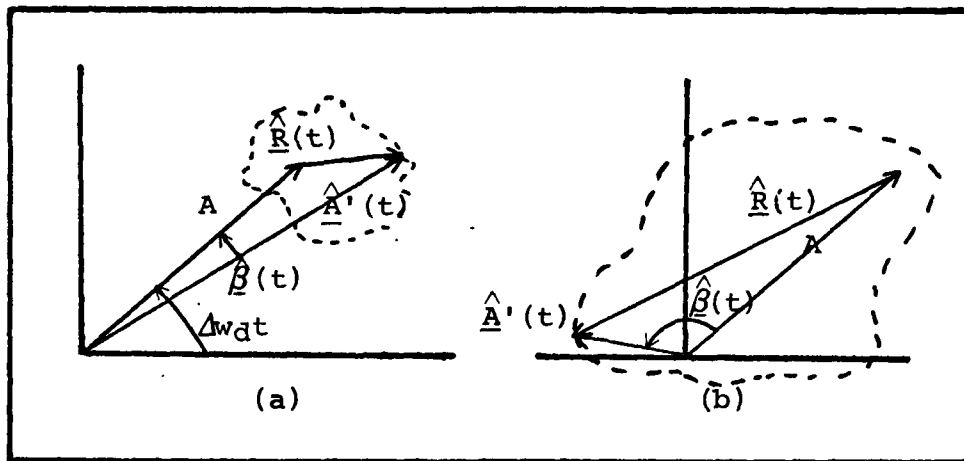


Figure 15. Phasor Diagram For Signal Plus Noise Prior to LD. (a) High CNR. (b) Low CNR.

With regard to Figure 15, a remark is warranted as to the direction of the encirclement. If no mistuning of the IF carrier was present (i.e., $\Delta\omega_d = 0$), the carrier phasor would be drawn parallel to the horizontal axis. Since the noise has a zero mean, the probability of a clockwise encirclement is the same as that for a counter clockwise encirclement. However, when the carrier is modulated, it has been found that the encirclement is favored in a direction opposite to the rotation of the carrier phasor (ref 16:250). In addition, the overall probability of either a clockwise or counterclockwise encirclement increases with the modulation.

An encirclement of the origin is characterized by a $\pm 2\pi$ rotation of the resultant phasor. The discriminator output voltage is based on the derivative of the carrier phase prior to the LD.

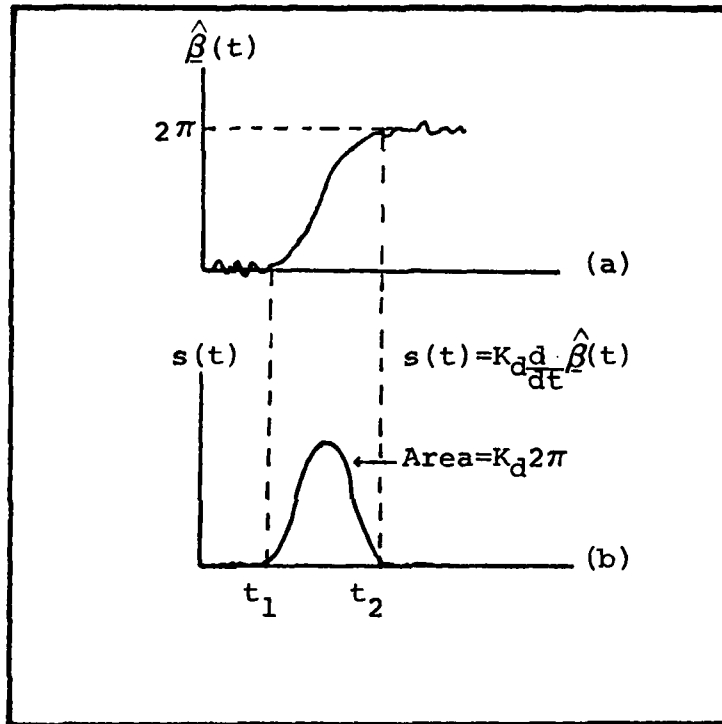


Figure 16. Equivalent Noise Phase at LD input (a) and Voltage Spike at LD output (b)

If the equivalent phase $\hat{\beta}(t)$ abruptly changes by $\pm 2\pi$ radians, either a positive or a negative voltage spike will result. For a positive shift in $\hat{\beta}(t)$, as in Figure 16a, a spike similar to that depicted in Figure 16b will be produced by the discriminator. The net area under the spike waveform $s(t)$ is $2\pi K_d$, where K_d is the discriminator gain in volts-sec/radian.

$$\begin{aligned}
\text{Spike area} &= K_d \int_{t_2}^{t_1} \frac{d\hat{\beta}(t)}{dt} dt & (58) \\
&= K_d \hat{\beta}(t) \Big|_{t_2}^{t_1} \\
&= K_d 2\pi
\end{aligned}$$

Bennet (ref 1:158) claims that in the FMFB, due to the feedback characteristics of the device, rapid phase variations prior to the LD are reduced to net phase excursions of $\frac{2\pi}{1+K}$, where K is the DC gain of the FMFB. Correspondingly, spikes of area $\frac{K_d 2\pi}{1+K}$ result. Since the velocity gate has the same structure as the FMFB, an equivalent spiking phenomenon will be assumed.

Recall the ultimate objective here is to determine the RMS deviation of the VCO frequency due to noise. Part of this deviation is due to linearly filtered equivalent phase noise at the input to the gate, given by Eq. (51). However, the actual deviation should be greater than this because the power contributed by the baseband voltage spikes has not been included. To this end, the power spectrum of the spike voltage must be found.

Because the spikes occur at random times and are impulse-like in character, they represent a shot noise phenomenon.

Taub and Schilling (ref 14:263) maintain the power spectral density of the spikes is

$$S_s(f) = N_s \overline{|F_s(j\omega)|^2} \quad (59)$$

where N_s is the number of spikes occurring per second and the averaging is performed over the squared magnitude of the Fourier transform of the spikes. Depicted in Figure 17 is an illustrative representation of this transform. Note its spectral width is confined to approximately half the bandwidth of the IF filter preceding the LD. This is so because the equivalent noise phase which produces the spikes is also confined to this bandwidth.

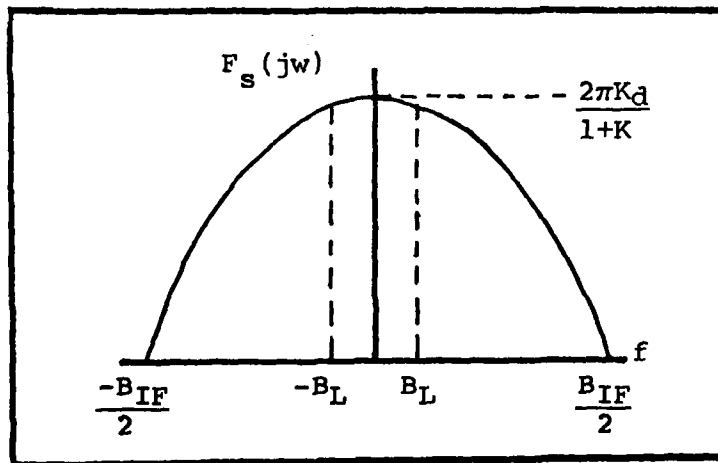


Figure 17. Typical Fourier Transform of Voltage Spike. (ref 14:324)

Indicated in Figure 17 is the relative extent of the bandwidth B_L of the low-pass filter following the LD. Within this band, the power density of the spikes can be considered constant at the value $N_s \overline{|F_s(0)|^2}$. If the waveform of a voltage spike is given by $s(t)$, and recalling that in the closed loop the area under the waveform is $\frac{2\pi}{1+K}$, the Fourier transform of $s(t)$ evaluated at $w = 0$ is

$$F_s(0) = \int_{-\infty}^{\infty} s(t) e^{-j2\pi(0)t} dt = \frac{2\pi K_d}{1+K} \quad (60)$$

In a bandwidth B_L , just prior to the VCO, the average power due to spikes will be

$$P_s = K_b^2 K_d^2 2B_L \frac{(2\pi)^2 N_s}{(1+K)^2} \quad (61)$$

$$= \frac{8\pi^2 K_b^2 K_d^2 B_L N_s}{(1+K)^2}$$

Here K_b is the gain of the baseband amplifier. Defining the voltage at the VCO input due to spikes as $V_s(t)$, its mean square value will thus be $E[V_s^2(t)] = P_s$. In response to $V_s(t)$, the VCO output frequency is

$$f_o(t) = K_v V_s(t) \quad (\text{due to spikes}) \quad (62)$$

where K_v is the VCO gain in $\frac{\text{radian}}{\text{sec-volt}}$. We can thus reach our

objective of expressing the mean squared VCO frequency deviation due to spikes as follows

$$\begin{aligned} E \left[f_o^2(t) \right] &= K_v^2 E \left[V_s^2(t) \right] \quad (\text{due to spikes}) \quad (63) \\ &= \frac{K^2 8\pi^2 B_L N_s}{(1+K)^2} \\ &= 8\pi^2 B_L N_s \quad K \gg 1 \end{aligned}$$

Here $K = K_v K_b K_d$.

It was mentioned earlier that the number of spikes per second increases as the CNR prior to the LD decreases. In addition, recall that any frequency deviation of the signal carrier from the IF center frequency causes an increase in the rate of spikes. These facts are inherent in the expression for N_s (ref 14:335-336), given by

$$N_s = \frac{B_{IF} \text{erfc} \sqrt{\text{CNR}_{IF}}}{2\sqrt{3}} + \overline{|\Delta f|} e^{-(\text{CNR}_{IF})} \quad (64)$$

The function "erfc" is defined in Eq. (47). The only unfamiliar term in Eq. (64) is $\overline{|\Delta f|}$, which is the average magnitude of the IF carrier frequency deviation. As a first approximation, from Eq. (55) assume $\overline{|\Delta f|} = \frac{\Delta \omega_d}{2\pi}$, the static

frequency tracking error.

The total mean square frequency deviation of the VCO can now be found by combining the contributions provided by the linearly filtered noise and spike noise. These are given by Eqs. (51) and (63) respectively. Referencing all CNR's to a bandwidth equal to the closed loop noise bandwidth requires the substitution $CNR_{IF} = \frac{2B_n}{B_{IF}} CNR_n$ (compare

Eqs. (44) and (56)). With this in mind, the net mean square VCO frequency deviation is

$$E[f_o^2(t)] = \frac{2\pi^2 B_n^2}{3 CNR_n} \quad (65)$$

$$+ 8\pi^2 B_L \left[\frac{B_{IF} \text{erfc} \sqrt{\frac{2B_n CNR_n}{B_{IF}}}}{2\sqrt{3}} + \overline{|\Delta f|} \exp\left(-\frac{2B_n CNR_n}{B_{IF}}\right) \right]$$

According to our definition, the velocity gate will reach its threshold when $f_o(\text{RMS}) = \frac{B_{IF}}{2}$.

Example

Consider an implementation of Eq. (65) in determining the threshold of a velocity gate with the following characteristics:

1. IF Baseband Equivalent $H_{LP}(j\omega) = \frac{\omega_1}{j\omega + \omega_1}$ (66)

$$\omega_1 = 2\pi \cdot \frac{B_{IF}}{2} = 2\pi \cdot 300 \text{ Hz}$$

2. Low Pass Filter $H_L(j\omega) = \frac{\omega_2}{j\omega + \omega_2}$ (67)

$$\omega_2 = 2\pi \cdot B_L = 2\pi \cdot 1 \text{ Hz}$$

3. The DC gain K is arbitrarily established here such that the maximum static frequency error in the IF filter is no greater than five percent of the filter's bandwidth. Recall from Section III that the static error exists in response to a constant doppler shift of the gate input carrier frequency. As defined above, the error is small enough to consider the net deviation of the IF carrier to be caused solely by noise. Reducing the static frequency error further means a higher DC gain is required,

which, as shown below, increases the noise bandwidth of the gate. Thus, the DC gain criterion is a compromise between a large noise bandwidth with small static frequency error and a large static frequency error with small noise bandwidth. Assuming the maximum doppler shift is 18 KHz, from Eq. (9) we have

$$K \approx \frac{18,000}{\Delta w_d} = \frac{18,000}{(.05)(600)} = 600 \quad (68)$$

4. From Eq. (21) the closed loop transfer function of the velocity gate with the above filter characteristics is

$$G(jw) = \frac{Kw_1w_2}{(jw)^2 + jw(w_1 + w_2) + w_1w_2(1 + K)} \quad (69)$$

5. With the closed loop transfer function expressed as a ratio of polynomials in jw , the noise bandwidth can be found with the aid of published tables (ref 7:21; 17:369,370). For the second order system defined by Eq. (69)

$$\begin{aligned} B_n &= \frac{Kw_1w_2}{4(w_1 + w_2)} \quad (70) \\ &= 149.5 \text{ Hz} \end{aligned}$$

The RMS frequency deviation $f_o(\text{RMS})$ of the VCO is given by the square root of the expression in Eq. (65). Figure 18 is a plot of the deviation versus CNR_n , the carrier-to-noise ratio in a bandwidth B_n , which is the closed-loop noise bandwidth. The solid line (curve (a)) is the plot corresponding to $\overline{|\Delta f|} = 30$ Hz. As a matter of interest, a plot of the frequency deviation due to just the linearly filtered input phase process overlays the solid line in Figure 18 without any significant difference. This implies that, at least for a small $\overline{|\Delta f|}$, and the particular velocity gate just defined, the noise spikes in the baseband are not contributing enough power to affect the RMS frequency deviation of the VCO in a significant manner.

Clearly, the noise will cause the average of the magnitude of the IF frequency deviation to be greater than 30 Hz. As CNR_n is lowered, $\overline{|\Delta f|}$ would tend to increase, thus requiring, in the general case, a new value for $\overline{|\Delta f|}$ with every computation of $f_o(\text{RMS})$. But for the present case, the spikes virtually do not affect the deviation of the VCO. This is indicated by the dashed line (curve (b)) in Figure 18, which is a plot of $f_o(\text{RMS})$ with $\overline{|\Delta f|} = 300$ Hz. We can see the VCO frequency deviation is due almost entirely to the first term in Eq. (65).

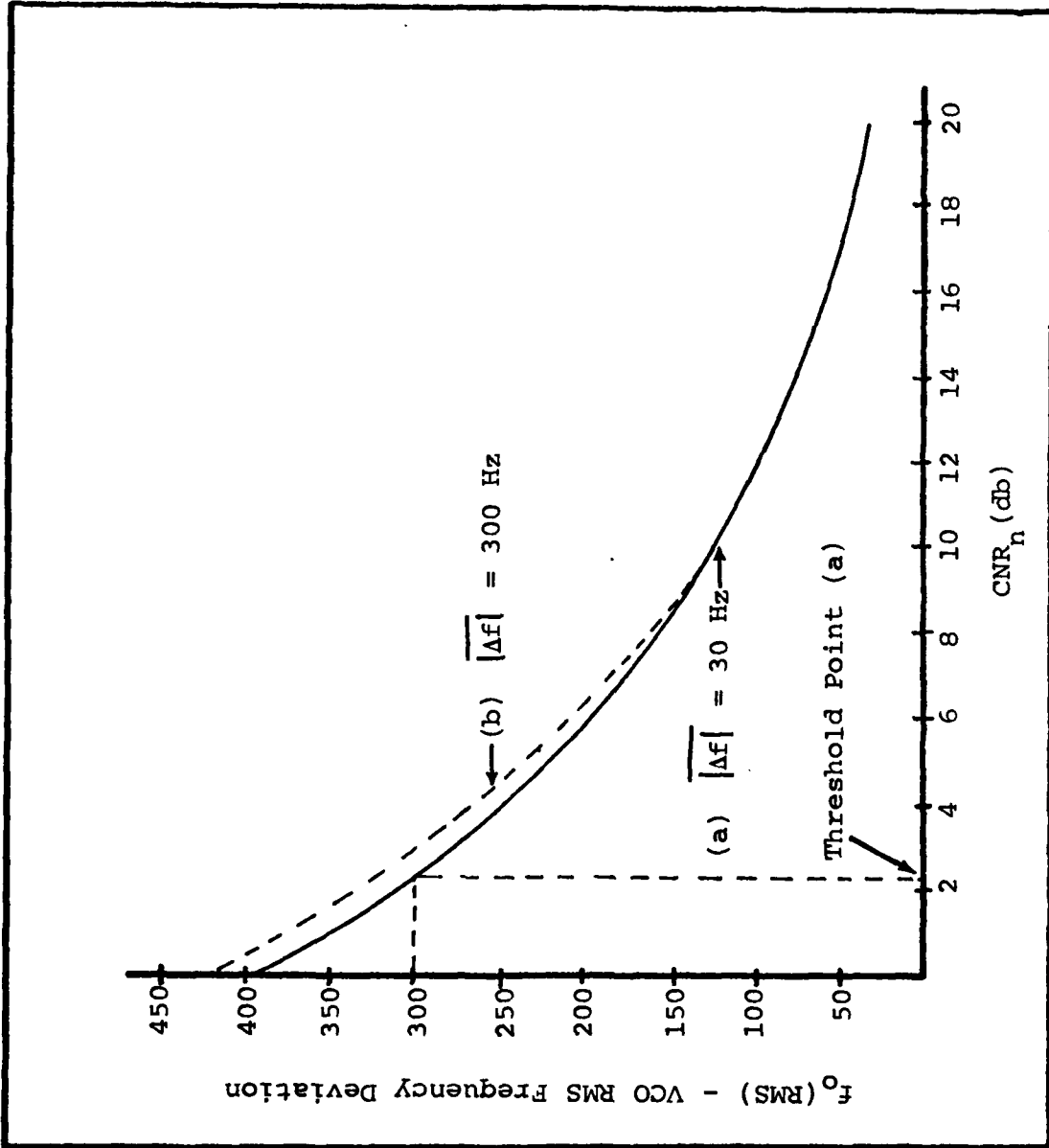


Figure 18. CNR_n vs VCO RMS Frequency Deviation Due To Noise

Alternate Definition of Threshold

Up to this point the emphasis has been placed on determining the RMS frequency deviation of the VCO due to noise. Defining the threshold in terms of a particular RMS deviation is helpful insofar as it provides a means of gauging the relative tracking performance of the velocity gate for various values of CNR. It has been maintained all along that if the scan-modulated IF carrier is pushed into the skirts of the IF filter due to a large tracking error, then the modulation is subject to excessive distortion. Yet, even if the RMS frequency deviation is large enough to push the modulation into the skirts, we are only assured the modulation will be there part of the time. Thus, it might be said that the gate moves in and out of its threshold state.

Some of the uncertainty regarding the actual tracking error can be removed by considering the probability that the error exceeds a certain amount as a function of CNR. If the statistics of the VCO frequency process $f_0(t)$ are known, it should be possible to quantify the performance of the gate in terms of a probability statement. The performance criterion would still be the frequency error in the IF filter. Consistent with the reasoning that "good" tracking occurs if the error is less than half the IF bandwidth, the threshold could be defined for any time t as the probability that

$\left[|f_o(t)| > \frac{B_{IF}}{2} \right]$ exceeds a predetermined value. Note this

definition assumes meaning when the input signal phase function is zero and the static tracking error in the IF is neglected. For under these circumstances, the IF frequency error is equal to the random VCO frequency.

Returning to the second order system in the example above, we can determine its performance based on the second threshold definition just presented. In general, the statistics of the VCO frequency process will be related to the characteristics of the two noise mechanisms which produce it - the linear filtering of the equivalent phase noise at the gate input and the baseband spike noise. However, recall from Figure 18 that the spike noise did not significantly contribute to the deviation of the VCO in the example. By avoiding any mention of the spikes, we can model the gate as a linear filter (see Eq. (50)), with the input being the equivalent phase noise process and output being the VCO frequency process. Since the input is Gaussian, zero mean and stationary, the output will be too.

At any particular time t the VCO frequency will be a random variable $f_o(t)$. Its variance $\sigma_{f_o}^2$ is given by Eq. (51),

$$\sigma_{f_o}^2 = E \left[\underline{f}_o^2(t) \right] \quad (71)$$

$$= \frac{2\pi^2 B_n^2}{3 \text{ CNR}_n}$$

Thus,

$$\text{probability} \left[\left| \underline{f}_o(t) \right| > \frac{B_{IF}}{2} \right] = 2 \int_{\frac{B_{IF}}{2}}^{\infty} \frac{1}{\sqrt{2\pi} \sigma_{f_o}} \exp \left[-\frac{1}{2} \left(\frac{f_o}{\sigma_{f_o}} \right)^2 \right] df_o \quad (72)$$

With the change of variable $y = \frac{f_o}{\sigma_{f_o}}$ we have

$$\text{probability} \left[\left| \underline{f}_o(t) \right| > \frac{B_{IF}}{2} \right] = 2 \int_{\frac{B_{IF}/2}{\sqrt{2} \sigma_{f_o}}}^{\infty} \frac{1}{\sqrt{\pi}} \exp \left[-y^2 \right] dy \quad (73)$$

$$= \text{erfc} \left(\frac{B_{IF}/2}{\sqrt{2} \sigma_{f_o}} \right)$$

$$= \text{erfc} \left(\frac{B_{IF} \sqrt{3}}{4\pi B_n} \sqrt{\text{CNR}_n} \right)$$

For the second order system introduced previously, with noise bandwidth $B_n = 149.5$ Hz and IF bandwidth $B_{IF} = 600$, a plot of Eq. (73) is shown in Figure 19.

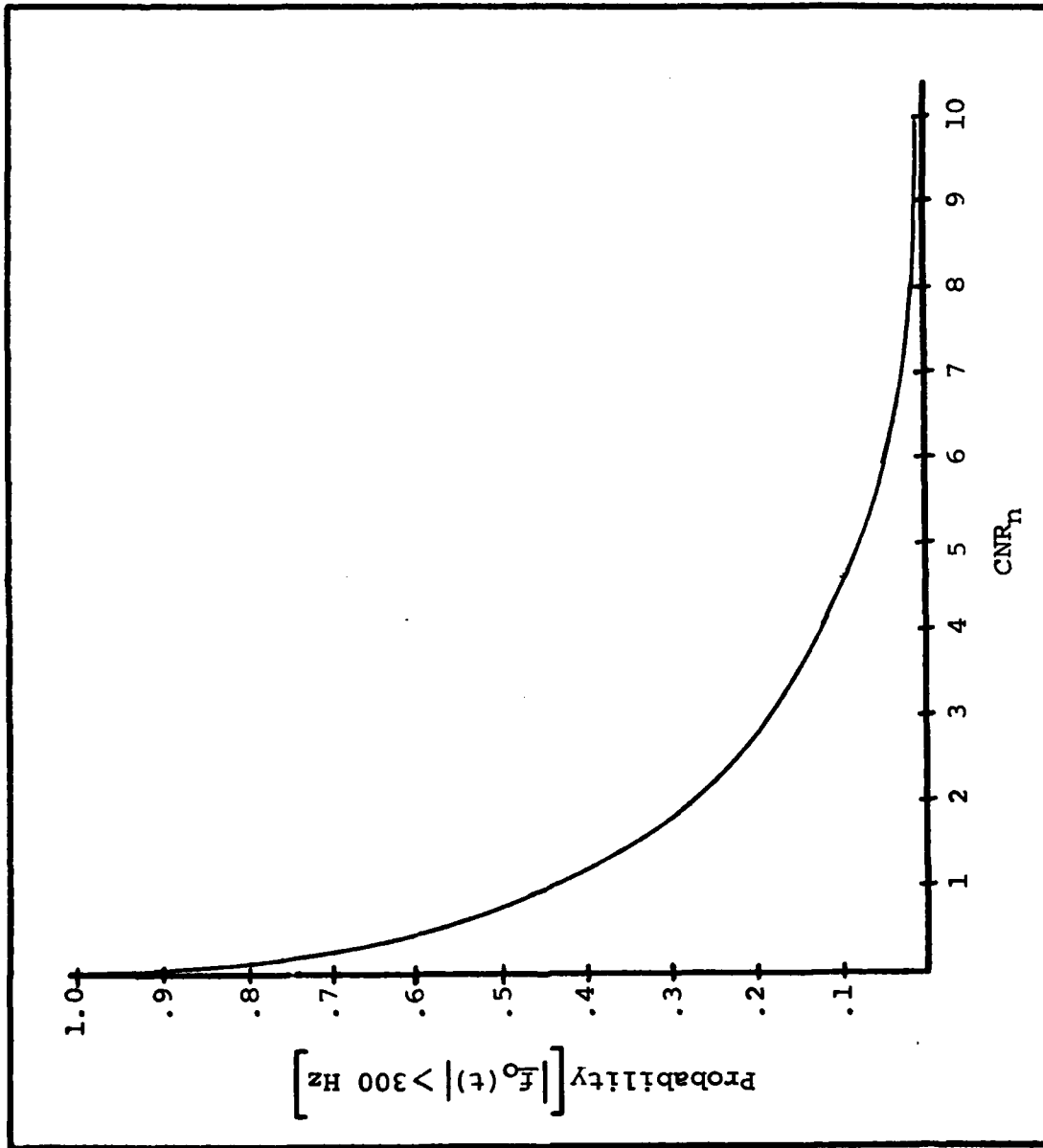


Figure 19. CNR_n vs Probability $[|f_0(t)| > 300 \text{ Hz}]$

From Figure 19 we can attach some additional meaning to the threshold CNR determined purely on the basis of the RMS deviation of the VCO frequency. According to Figure 18 the threshold of the system described in the example occurs at a CNR_n of about 2 db. This threshold was based on the definition that the RMS VCO deviation exceeds half the IF bandwidth at the threshold. However, from Figure 19, the probability the actual frequency deviation exceeds half the IF bandwidth, for $CNR_n \approx 2\text{db}$, is only about .28.

V. CONCLUSION

Summary

The objectives of this report have been 1) to determine a linear model of a velocity gate which predicts the frequency tracking behavior in the absence of noise and 2) to use the model to show how narrowband, Gaussian noise affects the tracking performance. By recognizing the similarity between the velocity gate and a frequency modulation feedback demodulator (FMFB), the analysis of the FMFB contained in the literature was adapted to reach the objectives at hand.

It is clear, however, that the criterion of performance for the velocity gate has to be uniquely defined. In the FMFB this criterion is the detected signal-to-noise ratio. However, since the purpose of the velocity gate is to maintain the scan-modulated IF carrier, within the passband of the gate's IF filter, a logical criterion of performance was stated to be the frequency tracking error within the IF filter. The implication of a large error is that the scan modulation is carried into the skirts of the IF filter, and is therefore subject to much more distortion than if it were within the passband. In addition, operation within the skirts of the IF can cause excessive variations in the phase of the

scan-modulated IF carrier, which can potentially make the gate unstable. Consistent with the IF frequency error criterion, two definitions for the threshold of the gate were suggested. One maintained that the threshold occurred when the RMS frequency error in the IF filter exceeded half the 3db bandwidth of the filter. The other based the threshold on the condition of the actual frequency error exceeding half the IF 3db bandwidth with a certain predetermined probability. The latter definition is more meaningful in the sense that it allows one to quantify what percentage of the time the gate is not tracking well, i.e., has lost lock on the input signal.

The linear model is based on the conditions of the phase and frequency tracking errors in the IF filter being small. Specifically, the phase error must be much less than one radian and the frequency error no more than half the IF bandwidth. Since the gate cannot distinguish between the signal and noise at its input, its tracking behavior was shown to be governed by superimposing the response due to each component alone. Thus, the VCO phase and frequency fluctuated randomly about the deterministic response due to the signal. Consequently, the net phase and frequency tracking errors increased as the carrier-to-noise ratio within the loop decreased.

Based on the statistics of the VCO phase, a criterion for the validity of the linear model was established on the probability that the phase error exceeds one radian. In

arriving at this probability, the equivalent input noise phase was assumed to be Gaussian, irrespective of the CNR. Yet, in reality, as the CNR approaches one, the statistics of the equivalent noise phase are not purely Gaussian. Nevertheless, the assumption allows one to benchmark the relative phase tracking performance of the gate for varying CNR.

In the general case, the VCO frequency deviation will be caused by two mechanisms. The first occurs as a result of using the transfer function of the linear model of the velocity gate to define a linear filter whose output is the VCO frequency process, and whose input is the equivalent noise phase process. For a large CNR this procedure is valid. However, the linear model does not predict the occurrence of noise spikes in the baseband portion of the gate. These spikes become significant when the CNR in front of the discriminator is low enough to cause rapid variations in the equivalent noise phase at this point in the gate. The net frequency deviation of the VCO is assumed to be due to the sum of the deviations caused by each mechanism acting alone.

The approach followed in this report has been to adapt the documented analysis on the FMFB to the particular characteristics of the velocity gate. However, it must be kept in mind that each device is intended to accomplish a differ-

ent task. The analysis presented here is certainly not unique, and there are bound to be other approaches towards an understanding of the velocity gate. Nevertheless, some insight has been presented and the foundation has been laid for further research and for a basis of comparison with other analyses.

Recommendation

The theory presented in this report should be validated either by experiment with an actual velocity gate, or, if more feasible, by the use of a computer simulation.

Bibliography

1. Bennet, W., M. Schwartz and S. Stein. Communications System and Techniques. New York: McGraw-Hill Book Company, Inc. 1966.
2. Billig, J. A. and D. L. Schilling. "A Comparison of the Threshold Performance of the Frequency Demodulator Using Feedback and the Phase Locked Loop". Record of the International Symposium On Space Electronics. Miami Beach, Florida, November 1965. 3-E1 to 3E-8.
3. Blanchard, A. Phase-Locked Loops: Application to Coherent Receiver Design. New York: John Wiley and Sons, Inc., 1976.
4. Braun, W. and W. C. Lindsey. "Acquisition Behavior of Coupled AGC and Phase-Locked Loop Systems". National Telecommunications Conference NTC 75, 30: 12-15.
5. Chaffee, J. G. "The Application of Negative Feedback Modulation Systems". Proceedings of the IRE 27, 317-331. 1939.
6. Enloe, L. H. "Decreasing the Threshold in FM By Frequency Feedback." Proceedings of the IRE, pp. 18-29, January 1962.
7. Frankle, J. T. and J. Klapper. Phase-Locked and Frequency-Feedback Systems. New York: Academic Press, 1972.
8. Gardner, F. M. Phase-Lock Techniques. New York: John Wiley and Sons, Inc., 1966.
9. Kliger, I. E. and C. F. Olenberger. "Phase-Lock Loop Jump Phenomenon in the Presence of Two Signals". IEEE Aerospace and Electronic Systems, 12: 55-63, January 1976.
10. Kliger, I. E. and C. F. Olenberger. "Effects of Automatic Gain Control on Phase-Locked Loop Behavior in the Presence of Interference". The Institute of Electrical and Electronics Engineers, 803-805, November 1976.

11. Papoulis, A. Probability, Random Variables, and Stochastic Processes. New York: McGraw-Hill Book Company, Inc., 1965.
12. Papoulis, A. The Fourier Integral and Its Applications New York: McGraw-Hill Book Company, Inc., 1962.
13. Sakrison, D. J. Communication Theory: Transmission of Waveforms and Digital Information. New York: John Wiley and Sons, Inc., 1968.
14. Schilling, D. and H. Taub. Principles of Communication Systems. New York: McGraw-Hill Book Company Inc., 1971.
15. Spilker, J. J., Jr. "Threshold Comparisons of Phase-Lock, Frequency-Lock and Maximum Likelihood Types of FM Discriminators". Western Electronic Show and Convention Record. San Francisco, August 1961.
16. Tranten, W. H. and R. E. Ziemer. Systems, Modulation and Noise. Boston: Houghton Mufflin Company, 1976.
17. James, H. M., N. B. Nichols and R. S. Phillips. Theory of Servomechanisms. New York: Mc Graw-Hill Book Company, Inc. 1947.

APPENDIX A

Response Of An IF Filter To A Mistuned Carrier

A bandpass or IF filter with center frequency f_{IF} will be shown to have an impulse response $h_{IF}(t)$ expressed as

$$h_{IF}(t) = 2\text{Re} \left[\tilde{h}_L(t) e^{j(\omega_{IF} + \Delta\omega_d)t} \right] \quad (\text{A-1})$$

$$\omega_{IF} = 2\pi f_{IF}$$

$$\Delta\omega_d = 2\pi\Delta f_d$$

Here $\tilde{h}_L(t)$ is a complex envelope referenced to the frequency $f_{IF} + \Delta f_d$. This particular form of the impulse response is convenient when dealing with modulated carriers that are offset or mistuned from the IF center frequency by Δf_d . As an application of (A-1) the response to the input

$$A(t)\sin(\omega_i t + \Delta\omega_d t + \phi_e(t)) \quad (\text{A-2})$$

(Eq. (12) in the text) will be shown analytically.

Since $h_{IF}(t)$ is a real function, its Fourier transform will be symmetrical about $f = 0$. For the sake of simplicity, let its magnitude and phase response be as shown in Figure

(A-1).

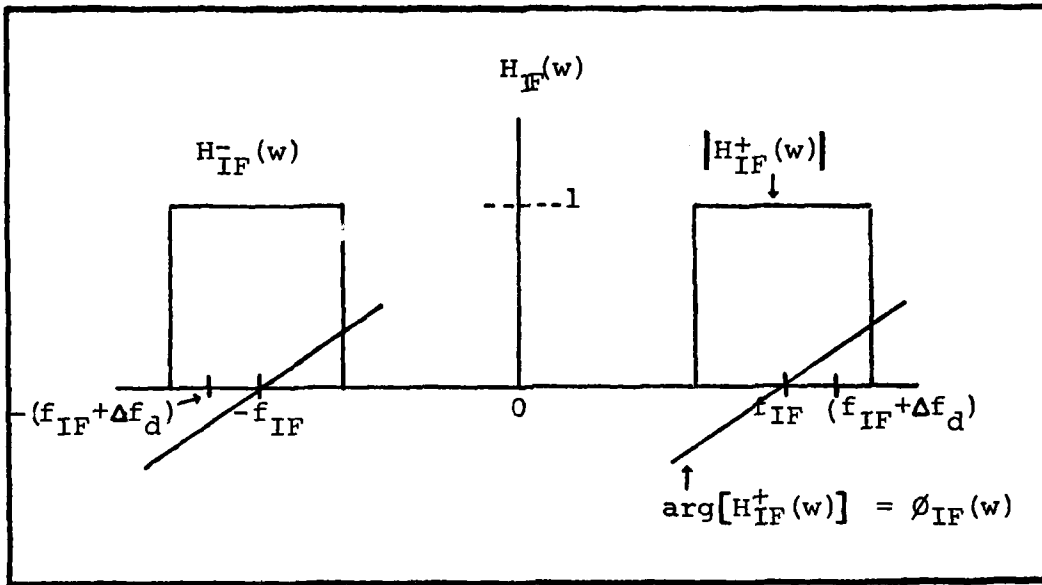


Figure A-1. Depiction of IF Filter Magnitude and Phase Responses

Note the transform has symmetrical positive and negative frequency components such that

$$H_{IF}(w) = H_{IF}^+(w) + H_{IF}^-(w) \quad (A-3)$$

Consider an IF input carrier frequency $f' = f_{IF} + \Delta f_d$. For such a carrier, which is off-centered in the IF passband by Δf_d , Papoulis (ref 11:131-134) derives an equivalent IF impulse response. The result is

$$h_{IF}(t) = 2h_p(t)\cos(w't) + 2h_q(t)\sin(w't) \quad (A-4)$$

The functions $h_p(t)$ and $h_q(t)$ are called the in-phase and quadrature system functions. They are defined by means of their Fourier transforms as follows

$$h_p(t) \leftrightarrow H_p(w) = \frac{H_{IF}^+(w + w') + H_{IF}^-(w - w')}{2} \quad (A-5)$$

$$h_q(t) \leftrightarrow H_q(w) = \frac{-H_{IF}^+(w + w') + H_{IF}^-(w - w')}{2j}$$

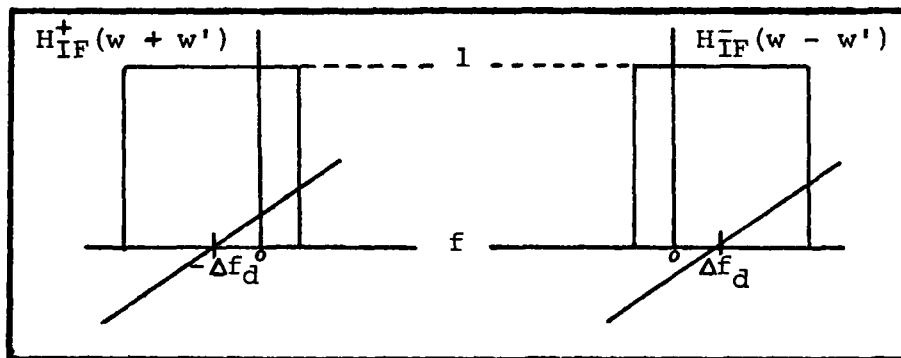


Figure A-2. Magnitude and Phase Responses of $H_{IF}^+(w + w')$ and $H_{IF}^-(w - w')$

Although $H_{IF}^+(w + w')$ and $H_{IF}^-(w - w')$ are complex due to their asymmetry about $f = 0$ (Figure A-2), when combined as in Eq. (A-5) they result in $H_p(w)$ and $H_q(w)$ being symmetrical and real. Note that for no mistuning, i.e. $f' = f_{IF}$, $H_q(w) = 0$. Function $H_p(w)$ is simply the passband response of the IF shifted and centered at $f = 0$.

From Eq. (A-4) the impulse response of the IF filter can be expressed in complex envelope form to yield Eq. (A-1).

Thus,

$$\begin{aligned} h_{IF}(t) &= 2\text{Re} \left[(h_p(t) - jh_q(t)) e^{jw't} \right] \\ &= 2\text{Re} \left[\tilde{h}_L(t) e^{jw't} \right], \end{aligned} \quad (\text{A-6})$$

where $\tilde{h}_L(t) = (h_p(t) - jh_q(t))$. The significance of this expression is that the IF filter's impulse response can be represented in a generalized complex envelope form. Referencing the envelope to the arbitrary frequency w' makes it convenient to find the filter's output to a mistuned carrier.

As an application of Eq. (A-6) consider a real narrow-band input signal of the form

$$\begin{aligned} s(t) &= x(t)\cos w't + y(t)\sin w't \\ &= \text{Re} \left[\tilde{s}(t) e^{jw't} \right] \end{aligned} \quad (\text{A-7})$$

where $\tilde{s}(t) = (x(t) - jy(t))$ is the complex envelope of $s(t)$. The Fourier transform of $s(t)$, like that of $h_{IF}(t)$ is comprised of distinct positive and negative portions, as shown in Figure A-3b. The output of the filter, shown in Figure A-3c, will be narrowband, which implies its bandwidth is sufficiently smaller than its mid-band frequency so the positive and negative frequency portions essentially do not overlap.

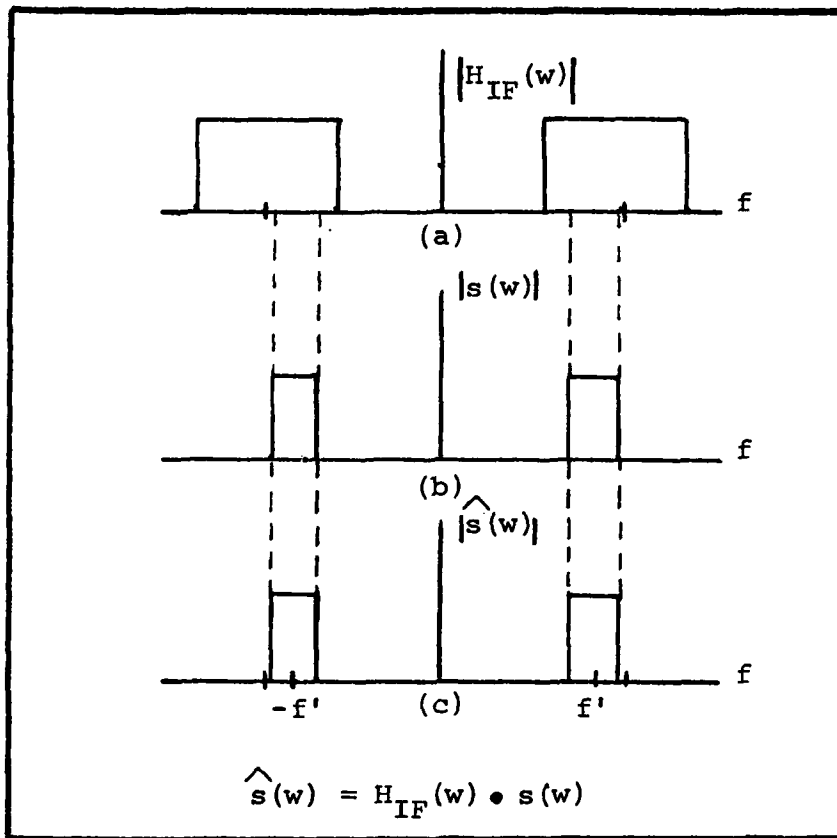


Figure A-3. Depiction of Narrowband Fourier Transforms of a) IF Filter Impulse Response $h_{IF}(t)$, b) IF Filter Input Signal $s(t)$, c) IF Filter Output Signal $\hat{s}(t)$

The convolution of $s(t)$ with $h_{IF}(t)$ to yield the filter output $\hat{s}(t)$ is written

$$\begin{aligned}
 \hat{s}(t) &= s(t) * h_{IF}(t) = 2\text{Re}\left[\tilde{h}_L(t)e^{jw't}\right] * \text{Re}\left[\tilde{s}(t)e^{jw't}\right] \quad (\text{A-8}) \\
 &= \text{Re}\left[(\tilde{h}_L(t) * \tilde{s}(t))e^{jw't}\right] \\
 &= \text{Re}\left[\hat{\tilde{s}}(t)e^{jw't}\right]
 \end{aligned}$$

Only when narrowband functions are involved can their convolutions be written using the convolutions of the envelopes.

The envelope of $s(t)$ is

$$\hat{s}(t) = \tilde{h}_L(t) * \tilde{s}(t) \quad (\text{A-9})$$

$$= (h_p - jh_q) * (x - jy)$$

$$= (h_p * x - h_q * y) - j(h_p * y + h_q * x)$$

Above, the designation (t) , meaning function of time, was omitted for clarity, as will be done hereafter where helpful. Using (A-9) in (A-8), the IF filter output is

$$\hat{s} = (h_p * x - h_q * y) \cos w't \quad (\text{A-10})$$

$$+ (h_p * y + h_q * x) \sin w't$$

Let us now consider the particular input given by Eq. (A-2) where we define $f_{IF} + \Delta f_d = f'$. Thus,

$$s(t) = A(t) \sin(w't + \phi_e(t)) \quad (\text{A-11})$$

$$= A(t) \sin \phi_e(t) \cos w't + A(t) \cos \phi_e(t) \sin w't$$

Comparing with (A-7) it is evident $x(t) = A(t) \sin \phi_e(t)$, and $y(t) = A(t) \cos \phi_e(t)$. The scan modulation $A(t)$ is considered so slowly varying that it is assumed it essentially

passes through the IF filter as if it were a constant. Hence, the IF output using (A-10) is

$$\hat{s}(t) = A(t)E(t)\sin(\omega't + \hat{\phi}_e(t)) \quad (A-12)$$

$$E(t) = \sqrt{(h_p * \sin \phi_e - h_q * \cos \phi_e)^2 + (h_p * \cos \phi_e + h_q * \sin \phi_e)^2}$$

$$\hat{\phi}_e(t) = \tan^{-1} \left[\frac{h_p * \sin \phi_e - h_q * \cos \phi_e}{h_p * \cos \phi_e + h_q * \sin \phi_e} \right]$$

Here, $E(t)$ is an envelope function, not to be confused with the envelope of the IF filter impulse response.

The above results may appear overwhelming and it may seem the IF filter distorts the scan modulation and input phase function more than anticipated. But a careful appraisal of what the functions h_p and h_q really mean will show the output of the filter is what would be expected. For example, if the mistuning of the IF carrier is kept within the filter's 3db bandwidth, we could argue the modulation, both amplitude and phase lie in the essentially flat portions of the IF passband. System functions $H_p(\omega)$ and $H_q(\omega)$ help describe in the baseband realm that which occurs at IF. Recall $H_p(\omega)$ is the sum of two shifted versions of the IF filter passband response and $H_q(\omega)$ is their difference (see Figure A-2 and

Eq. (A-4)). With slight mistuning and about $f=0$, $H_p(w) \gg H_q(w)$. Narrowband modulation centered at $f=0$ would then encounter a nonzero, essentially flat response due to $H_p(w)$ and a practically zero response for $H_q(w)$. If the mid-band IF gain is one, then $H_p(w) \approx 1$ around $f=0$. Therefore the envelope defined in Eq. (A-12) is

$$E(t) \approx \sqrt{(\sin^2 \phi_e + \cos^2 \phi_e)} = 1$$

and the phase response is

$$\phi_e(t) \approx \tan^{-1} \left[\frac{\sin \phi_e}{\cos \phi_e} \right] = \phi_e$$

These are expected results for perfect filtering.

It is evident that the extent of mistuning, the shape of the IF passband response and the bandwidth of the modulation all contribute to how "perfectly" an IF filter will pass an input. The analysis of systems incorporating an IF or bandpass filter is indeed simplified by assuming the filter induces no distortion. The results of this appendix provide an analytical understanding to justify such an assumption.

APPENDIX B

Derivation Of The Baseband Equivalent Of An IF Filter

The linear model of the velocity gate presented in Figure 5 incorporates a baseband representation of the IF filter. This representation, in effect, is an equivalent filter that has the same phase modulation response as the IF filter. However, as shown here, this representation is accurate when the modulation is much smaller than one radian. In addition, its accuracy increases the less the phase modulated IF input carrier is mistuned from the IF center frequency.

Before deriving the baseband equivalent filter, preliminary modifications need to be made to certain expressions in Appendix A. We now introduce the functions $h_p'(t)$ and $h_q'(t)$ which are defined by means of their Fourier transforms as follows.

$$h_p'(t) \leftrightarrow H_p'(w) = \frac{H_1(w) + H_2(w)}{2} \quad (B-1)$$

$$h_q'(t) \leftrightarrow H_q'(w) = \frac{-H_1(w) + H_2(w)}{2j}$$

where, referring to Figure (A-1)

$$H_1(w) = H_{IF}^+(w + w') e^{-j\phi_{IF}(w')} \quad (B-2)$$

$$H_2(w) = H_{IF}^-(w - w') e^{j\phi_{IF}(w')}$$

$$w' = 2\pi f' = w_{IF} + \Delta w_d$$

The only difference between $H_p'(w)$, $H_q'(w)$ and $H_p(w)$, $H_q(w)$ defined in Eq. (A-5) is the presence of the indicated phase shifts. Phase function $\phi_{IF}(w)$ corresponds to the phase response of the IF filter. It is a real function in the sense $(\phi_{IF}(w))^* = (-\phi_{IF}(-w))$ (ref 11:11), where the raised asterisk implies conjugation. The same argument Papoulis uses to show $H_p(w)$ and $H_q(w)$ are real (ref 11:132) can be used to show $H_p'(w)$ and $H_q'(w)$ are real. Later on, the significance of these phase shifts will be apparent. Based on Figure A-2, the functions $H_1(w)$ and $H_2(w)$ can be depicted as in Figure B-1. The important aspect to note about $H_1(w)$ and $H_2(w)$ is that their phase responses at $f = 0$ are equal to zero.

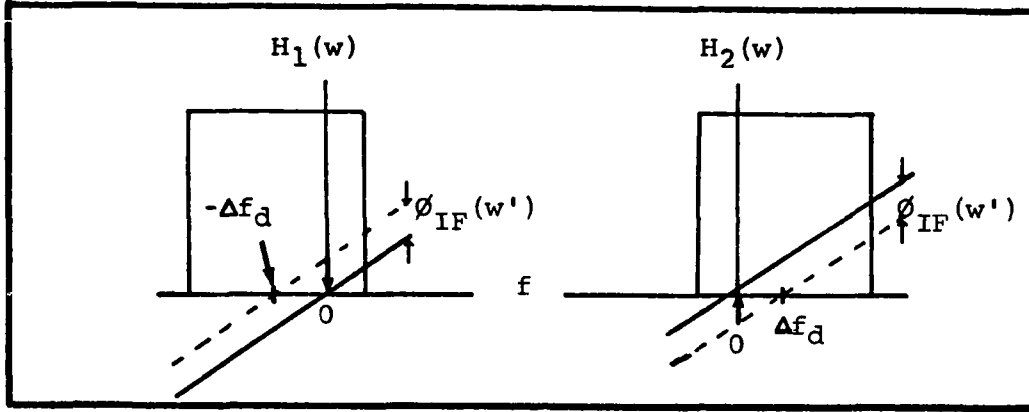


Figure B-1. Magnitude and Phase Responses of $H_1(w)$ and $H_2(w)$

The important aspect to note about $H_1(w)$ and $H_2(w)$ is that their phase responses at $f = 0$ are equal to zero.

We now show that the IF filter envelope given in Eq. (A-6) as $\tilde{h}_L(t) = (h_p(t) - jh_q(t))$ is expressible in terms of $h_p'(t)$ and $h_q'(t)$. Note from applying Eqs. (B-1) and (B-2)

$$H_p'(w) - jH_q'(w) = H_{IF}^\dagger(w + w') e^{-j\phi_{IF}(w')} \quad (B-3)$$

Using Eq. (A-5) we can equate the following

$$\begin{aligned} \tilde{H}_L(w) &= H_p(w) - jH_q(w) = H_{IF}^\dagger(w + w') \\ &= (H_p'(w) - jH_q'(w)) e^{j\phi_{IF}(w')} \end{aligned} \quad (B-4)$$

Therefore, since $\phi_{IF}(w')$ is constant for constant w' ,

$$\tilde{h}_L(t) = h_p(t) - jh_q(t) = (h_p'(t) - jh_q'(t))e^{j\phi_{IF}(w')} \quad (B-5)$$

Consequently, the IF filter impulse response can be written in terms of $h_p'(t)$ and $h_q'(t)$ by substituting Eq. (B-5) into Eq. (A-6). The result is

$$h_{IF}(t) = 2\text{Re} \left[(h_p'(t) - jh_q'(t))e^{j\phi_{IF}(w')} e^{jw't} \right] \quad (B-6)$$

The same procedure followed in Appendix A can be used here to find the response of the IF filter to a mistuned carrier.

However, the output envelope and phase function will, of course be dependent on the function $h_p'(t)$ and $h_q'(t)$. In addition, the output will contain a constant phase shift due to $\phi_{IF}(w')$.

Hence, for the input

$$s(t) = A(t)\sin(w't + \phi_e(t)) \quad (B-7)$$

the corresponding output will be

$$\hat{s}(t) = A(t)E'(t)\sin(w't + \phi_{IF}(w') + \hat{\phi}_e'(t)), \quad (B-8)$$

where,

$$E'(t) = \sqrt{(h_p' * \sin \phi_e - h_q' * \cos \phi_e)^2 + (h_p' * \cos \phi_e + h_q' * \sin \phi_e)^2}$$

$$\hat{\phi}_e'(t) = \tan^{-1} \left[\frac{h_p' * \sin \phi_e - h_q' * \cos \phi_e}{h_p' * \cos \phi_e + h_q' * \sin \phi_e} \right]$$

where h_p' , h_q' and ϕ_e are understood to be functions of time.

As mentioned above, the linear model of the velocity gate is based upon the condition that the phase error before the IF filter is small. This implies the gate is tracking the input phase pretty well. The basis for this small-phase criterion lies with the approximation

$$\sin \phi_e(t) \approx \phi_e(t) \quad (\text{B-9})$$

$$\text{for } |\phi_e(t)| \ll 1$$

$$\cos \phi_e(t) \approx 1$$

If the approximations can be justified, several simplifications arise in the expressions for $E'(t)$ and $\hat{\phi}_e'(t)$ in

Eq. (B-8). These are

$$h_p' * \sin \phi_e = h_p' * \phi_e \quad (\text{B-10})$$

$$h_p' * \cos \phi_e = h_p' * 1 = H_p'(0) \quad (\text{B-11})$$

$$h_q' * \sin \phi_e = h_q' * \phi_e \quad (B-12)$$

$$h_q' * \cos \phi_e = h_q' * 1 = H_q'(0) \quad (B-13)$$

Note from Eq. (B-1) and Figure B-1 that $H_q'(0) = 0$ and $H_p'(0)$ is real (the reason for the phase shifts in Eq. (B-2) should now be apparent).

Based on the above approximations we can now write

$$E'(t) = \sqrt{(h_p'(t) * \phi_e(t))^2 + (H_p'(0) + h_q'(t) * \phi_e(t))^2} \quad (B-14)$$

$$\hat{\phi}_e'(t) = \tan^{-1} \left[\frac{\phi_e(t) * h_p'(t)}{H_p'(0) + \phi_e(t) * h_q'(t)} \right]$$

A further argument can be used to justify $H_p'(0) \gg \phi_e(t) * h_q'(t)$ and $H_p'(0) \gg \phi_e(t) * h_p'(t)$. Recall from Eq. (B-1) and Eq. (B-2) that $H_p'(w)$ is defined by the sum of two shifted versions of the IF passband response and $H_q(w)$ by the difference. For a carrier offset, Δf_d , well within half the 3db bandwidth of the IF filter, $H_p'(w)$ will be much greater than $H_q'(w)$ in a region about $f = 0$. Notice for $f = 0$, $H_q'(w) = 0$. Indeed, one of the considerations in the design of the velocity gate is the maintenance of the smallest possible static frequency tracking

AD-A080 411

AIR FORCE INST OF TECH WRIGHT-PATTERSON AFB OH SCHOO--ETC F/8 17/9
THRESHOLD OF THE VELOCITY GATE IN A CONTINUOUS WAVE RADAR WITH --ETC(U)
DEC 79 J P SUNRAY
AFIT/02/EE/79-88

UNCLASSIFIED

NL

2 of 2

AD-A080 411



END

DATE

TO REG

3 - 80

BT

error (given by Δf_d in the analysis of this report) within the IF filter. To minimize distortion of the scan modulation and prevent operation within the skirts of the IF filter, the maximum static frequency error is likely to be well within half the filter's 3db bandwidth. Therefore, with $H_p'(w)$ generally much greater than $H_q'(w)$, and with $|\phi_e(t)| \ll 1$ we can justify

$$H_p'(0) \gg \phi_e(t) * h_q'(t) \quad (B-15)$$

$$H_p'(0) \gg \phi_e(t) * h_p'(t)$$

The expressions in Eq (B-14) further simplify to

$$E'(t) = H_p'(0) \quad (B-16)$$

$$\hat{\phi}_e'(t) = \phi_e(t) * \frac{h_p'(t)}{H_p'(0)}$$

where the approximation $\tan^{-1}(x) \approx x$ for $x \ll 1$ has been used above.

Recalling $\phi_e(t)$ is the phase modulation of the IF input carrier and $\hat{\phi}_e'(t)$ the output modulation, we see the IF base-band equivalent is real and defined by the impulse response

$$h_{LP}(t) = \frac{h_p'(t)}{H_p'(0)} \quad (B-17)$$

How is $h_{LP}(t)$ related to the complex envelope of the IF filter, $\tilde{h}_L(t)$? From Eq. (B-5) it is evident

$$h_p'(t) = \text{Re} \left[\tilde{h}_L(t) e^{-j\phi_{IF}(w')} \right] \quad (\text{B-18})$$

and since $H_q(0) = 0$, from Eq. (B-4)

$$H_p'(0) = \tilde{H}_L(0) e^{-j\phi_{IF}(w')} \quad (\text{B-19})$$

where $H_p'(0)$ is real. Therefore

$$h_{LP}(t) = \text{Re} \left[\frac{\tilde{h}_L(t)}{\tilde{H}_L(0)} \right] \quad (\text{B-20})$$

In summary, a real baseband equivalent filter exists for an IF filter such that both have the same response to phase modulation. The equivalent filter is accurate when the modulation is much less than one radian and carrier mistuning is kept within the 3db bandwidth of the IF carrier.

VITA

Jonathan Paul Sunray was born on 14 May 1956 in Willemstad, Curacao, Netherlands Antilles. He graduated from The American High School, Mexico City, Mexico, in June 1974 and entered Rensselaer Polytechnic Institute, Troy, New York, in September 1974. Upon graduation from RPI in May 1978 with a Bachelor of Science in Electrical Engineering, he received the commission of second lieutenant in the United States Air Force. In June 1978 he entered the graduate program in Electrical Engineering at the Air Force Institute of Technology, Wright-Patterson Air Force Base, Ohio. Lieutenant Sunray was married to the former Shiela Darlage on 10 June 1979.

Permanent address: 1910 Washington Street
Columbus, Indiana 47201

UNCLASSIFIED

SECURITY CLASSIFICATION OF THIS PAGE (When Data Entered)

REPORT DOCUMENTATION PAGE		READ INSTRUCTIONS BEFORE COMPLETING FORM
1. REPORT NUMBER AFIT/GE/EE79-35	2. GOVT ACCESSION NO.	3. RECIPIENT'S CATALOG NUMBER
4. TITLE (and Subtitle) Threshold of the Velocity Gate in a Continuous Wave Radar With Conical Scan Tracking		5. TYPE OF REPORT & PERIOD COVERED MS Thesis
		6. PERFORMING ORG. REPORT NUMBER
7. AUTHOR(s) Jonathan P. Sunray 2Lt USAF		8. CONTRACT OR GRANT NUMBER(s)
9. PERFORMING ORGANIZATION NAME AND ADDRESS (AFIT/EN) Air Force Institute of Technology Wright-Patterson AFB, Ohio 45433		10. PROGRAM ELEMENT, PROJECT, TASK AREA & WORK UNIT NUMBERS
11. CONTROLLING OFFICE NAME AND ADDRESS Electronic Warfare Division - Aeronauti- cal Systems Division ASD/ENADD Wright Patterson AFB, Ohio 45433		12. REPORT DATE December 1979
		13. NUMBER OF PAGES 98
14. MONITORING AGENCY NAME & ADDRESS (if different from Controlling Office)		15. SECURITY CLASS. (of this report) UNCLASSIFIED
		15a. DECLASSIFICATION/DOWNGRADING SCHEDULE
16. DISTRIBUTION STATEMENT (of this Report) Approved for public release distribution unlimited.		
17. DISTRIBUTION STATEMENT (of the abstract entered in Block 20, if different from Report)		
18. SUPPLEMENTARY NOTES Approved for public release: distribution unlimited JOSEPH P. HIPPS, Major, USAF IAW AFR 190-17 Director of Information		
19. KEY WORDS (Continue on reverse side if necessary and identify by block number) Velocity Gate Threshold Conical Scan Angle Tracking Breaklock		
20. ABSTRACT (Continue on reverse side if necessary and identify by block number) A study is made of the behavior of the velocity gate in a continuous wave radar with conical scan tracking. Adapting the analysis of the frequency modulation feedback demodulator (FMFB), two linear models are developed for the velocity gate. The first deals with the gate's response to a static sopleter frequency offset and the second deals with its response to		

DD FORM 1473 1 JAN 73 EDITION OF 1 NOV 68 IS OBSOLETE

SECURITY CLASSIFICATION OF THIS PAGE (When Data Entered)

UNCLASSIFIED

SECURITY CLASSIFICATION OF THIS PAGE(When Data Entered)

a varying doppler frequency. The dynamic model also incorporates the presence of narrowband, Gaussian noise at the input to the gate. The phase tracking error of the gate due to noise is determined as a function of the carrier-to-noise ratio (CNR) in a bandwidth equal to the closed-loop noise bandwidth. Establishing the performance criterion to be the frequency tracking error, two definitions for the threshold of the gate are established. The first states the threshold occurs at the value of CNR for which the root-mean-square frequency tracking error due to noise exceeds half the 3db bandwidth of the IF filter within the gate. The second bases the threshold on the probability of the frequency error exceeding half the 3db bandwidth of the IF filter. Both definitions are applied to an example in which a second order velocity gate is considered.

SECURITY CLASSIFICATION OF THIS PAGE(When Data Entered)